Passively Mode-Locked Picosecond Nd:KGW Laser with Low Quantum Defect Diode Pumping

By

Md. Zubaer Eibna Halim

A thesis submitted to Faculty of Graduate Studies of
The University of Manitoba
In partial fulfillment of the degree of

MASTER OF SCIENCE

Department of Electrical and Computer Engineering
University of Manitoba
Winnipeg

Abstract

Solid-state lasers are capable of providing versatile output characteristics with greater flexibility compared to other popular laser systems. Lasing action has been achieved in many hundreds of solid-state media, but Nd-ion doped gain media are widely used to reach high power levels with short pulses.

In this work, commercially available Nd:KGW crystal served as a gain medium to achieve pulsed operation at 1067 nm. This laser crystal offers large stimulated emission cross-section and gain bandwidth which facilitates generation of high peak power pulses in the picosecond regime. The KGW crystal is monoclinic and biaxial in structure, and anisotropic in its optical and thermal properties. Due to poor thermal conductivity, this crystal can be operated within a limited power range before crystal fracture takes place. To reduce the amount of heat deposited in the gain media, we introduced a new pumping wavelength of 910 nm which reduces the quantum defect by more than 45%.

Continuous-wave laser operation was optimized to operate in mode-locked regime. In order to achieve short light pulses from the continuous-wave laser, one of the end mirrors was replaced by a semiconductor saturable absorber mirror (SESAM) to generate 2.4 ps pulses at a repetition rate of 83.8 MHz. An average output power of 87 mW was obtained at lasing wavelength of 1067 nm and the beam was nearly diffraction limited with $M^2 < 1.18$. The peak power of the generated pulses was 427 W and energy of each pulse was >1 nJ. Pumping the crystal at longer wavelength (910 nm) reduced the thermal lensing of the crystal by half when compared to conventional pumping at shorter wavelength (808 nm). To the best of our knowledge, this is the first time passive mode-locking of a Nd:KGW laser was explored using the pump wavelength at 910 nm.

Acknowledgements

I am deeply grateful to our supervisor Dr. Arkady Major. Over the last two years he has always guided us towards right direction and supported us with new ideas and technical solutions.

Throughout the course of experiment Tanant Waritanant, PhD candidate under Dr. Major's supervision has been extensively helpful. He is one of the smartest characters that I have ever come across. I would also like to thank Reza Akbari and Rubel Chandra Talukder. Reza helped me to get through theoretical ambiguities and introduced me with experimental systems. Rubel motivated me to cut decent figures in the courses and maintain good research esteem to successfully achieve experimental goals. My other groupmates Sujith, Shirin, Anvar and Chandan has supported me to keep high spirit.

I would also like to thank the members of my committee, Prof. Sherif Sherif and Prof. Olanrewaju Ojo for taking the time to review my thesis and participate in my defense.

Table of content

List of figures

List of tables

List of abbreviations

Laser	Light amplification by stimulated emission of radiation
DPSSL	Diode-pumped solid-state laser
FWHM	Full width at half maximum
QD	Quantum defect
CW	Continuous-wave
CWML	Continuous-wave mode-locking
SESAM	Semiconductor saturable absorber mirror
APM	Additive pulse mode-locking
KLM	Kerr lens mode-locking
SRS	Stimulated Raman scattering
AR	Antireflection
HR	High reflection
OC	Output coupler
SHB	Spatial hole burning
CCM	Cubic centimeter per minute
SAM	Self-amplitude modulation

Chapter 1 Introduction

1.1 Introduction

The foundation of '*Laser*' was laid by Albert Einstein when he introduced the idea of stimulated emission. In 1960, Theodore Maiman developed the first working laser based on Ruby [1]. Now laser light has become a vital part in data storage technologies, eye surgery, cancer treatment and micromachining – while once the innovator described it as 'a solution looking for problem'. '*Maser*'- stands for Microwave Amplification by Stimulated Emission of Radiation, similar to the working principle of lasers, was developed earlier in 1954.

There are different kinds of lasers operating from ultraviolet to far infrared spectral region, e.g. gas lasers, chemical lasers, dye/ liquid lasers, solid-state lasers and semiconductor lasers. Among these types, solid-state lasers are extensively investigated because they offer nearly diffraction limited beam quality along with high efficiency.

Mode-locked lasers generate very short pulses of light. These short light pulses are the key to explore the dynamic behavior of matter on ever-shorter timescales e.g. chemical reaction. Over the last decade the number of applications of ultra-short light pulses has skyrocketed and include such different areas as nonlinear frequency conversion [2, 3, 4, 5] nonlinear microscopy [6], nonlinear [7] and time-resolved [8] spectroscopy. Ahmed Zewail won Noble Prize in Chemistry in 1999 by demonstrating measurement of the rate of vibrational-energy redistribution for an isolated molecule using a picosecond laser [9]. Often light pulses are so short that there was a time when scientists were capable of generating ultrashort pulses, but the state-of-art for measuring the exact parameters of such light pulses was not available. This field of optics has advanced so far that researchers have developed laser systems that can generate attosecond (1 as = 10^{-18} s) pulses, which is close to its natural limit

[10]. Wave cycle lasts somewhat longer than one femtosecond (1 fs = 10^{-15} s) in the visible spectral range. High time and spatial resolution, large bandwidth and potential for high intensity offered by ultrashort pulses can be useful in numerous applications. Commercial products available for ophthalmic surgery, tattoo or unwanted hair removal, range finder, atmospheric CO_2 level monitoring, laser cutter are based on proficient application of mode-locked laser pulses.

1.2 Objectives

Neodymium-doped crystals are famous for efficiently producing short pulses with excellent beam quality. Among the various Nd-doped crystals, the crystal of Nd-doped potassium gadolinium tungstate [Nd:KGd$(WO_4)_2$, Nd:KGW] is well-known for continuous-wave (CW) [11], Q-switched [12] and mode-locked operation [13, 14]. This crystal is also known as PGT (Potassium Gadolinium Tungstate) in literature. The goal of the experiment was to study lasing operation of Nd-doped KGW crystal in continuous-wave mode-locked regime. The main three items of the system were:

- *Pumping Source* – A fiber coupled laser diode providing optical power to 'active medium'
- *Active Medium* – Nd-doped KGW crystal, absorbs pump power and provides optical gain to compensate losses
- *Optical Resonator* – A five mirror cavity in which laser radiation circulates and passes through active medium and where semiconductor saturable absorber mirror was used as one of the end mirrors to generate ultrashort pulses of light.

Under diode-pumped lasing operation, the main reasons for heat deposition in the active/gain medium are:

- Quantum Defect (QD), defining energy difference in between the pump photon and the lasing photon. In general, the lasing wavelength is longer compared to the pump wavelength, which implies that pump photon energy is higher than that of lasing photon. This energy difference of the pump and laser photons is lost as heat to the host lattice, as shown in figure 1.1.

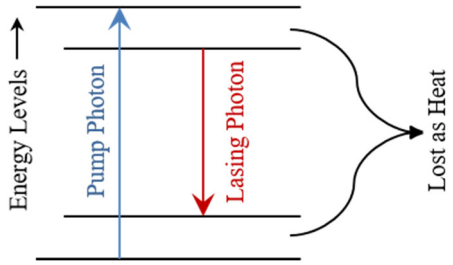

Figure 1.1: Quantum defect in a 4-level laser system.

- Non-radiative relaxation from the upper laser level to ground state due to concentration quenching and non-radiative relaxation from the pump band to the ground state [15].

Nd:KGW crystal supersedes many popular laser crystals in terms of optical parameters but its thermal conductivity disfavors the crystal to be operated in high power regime. Combined thermo-optic and stress-induced refractive index difference within Nd:KGW leads to the generation of an astigmatic thermal lens [16]. To address this issue, we pumped the crystal at longer pumping wavelength to reduce the energy difference between the pump and lasing photons, i.e. the QD. At the same time the absorption cross-section for the corresponding pump wavelength was not significant. To compensate for this issue in the experiment a relatively long crystal was utilized. For loss modulation in the cavity to lock the phases of the amplified optical frequency modes, a semiconductor saturable absorber mirror (SESAM) was equipped.

1.3 Motivation

This laser crystal has strong polarized emission lines at 1067 nm (corresponds to $^4F_{3/2} \rightarrow {}^4I_{11/2}$; $\sigma_{em}= 3.4x10^{-19}$ cm^2) and 1350 nm (corresponds to $^4F_{3/2} \rightarrow {}^4I_{13/2}$; $\sigma_{em} = 0.82x10^{-19}$ cm^2) [17]. High third-order nonlinearity of the host [18, 19, 20] along with high Raman gain coefficient makes this crystal attractive as Raman converter to realize eye-safe spectral range at 1537 nm [21]. In comparison with other popular gain media Nd:KGW offers higher stimulated emission cross-section than Nd:YAG (i.e. higher possibility of stimulated emission to take place) and broader gain bandwidth than Nd-doped YLF or YVO_4 (i.e. wider range of optical frequencies for amplification ensuring many modes to be locked in mode-locked operation). This makes it particularly suitable for generation of ultrashort pulses. Its relatively short upper-state lifetime (110 μs at 3% doping) results in reduced tendency towards self-Q-switching dynamics [22]. At the same time this monoclinic biaxial crystal exhibits strong anisotropy in its optical and thermal characteristics. Its thermal conductivity is 2.6, 3.8 and 3.4 $Wm^{-1}K^{-1}$ along the [100], [010] and [001] according to [23].

Recently it was shown that quantum defect in Nd:KGW can be significantly reduced (>45%) by using a hot-band pumping technique at ~910 nm [24]. In this case the electrons are excited from the thermally populated highest sublevel (i.e. hot-band) of the ground state manifold directly into the emitting laser level. This concept is illustrated in the following figure 1.2 showing the energy levels of Nd-ion in KGW matrix. Traditional pumping scheme around 810 nm as well as lasing transitions at 1067 nm and 1350 nm are shown along with the implemented low quantum defect hot-band pumping transition around 910 nm [24]. This excitation scheme has the lowest possible quantum defect in this particular system. Another possibility of low quantum defect pumping would be a direct in-band transition around 880 nm [25] corresponding to the excitation of an electron from the ground state to the emitting laser

level $^4F_{3/2}$. In this case, however, the quantum defect will be larger than for the pumping wavelength around 910 nm.

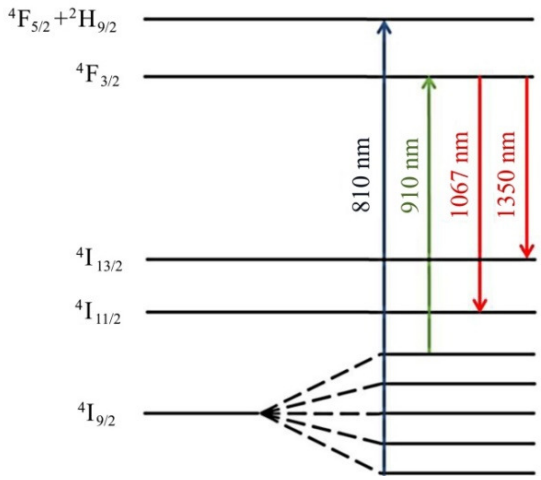

Figure 1.2: Energy level diagram of Nd:KGW crystal.

For these reasons, this work was aimed to achieve stable mode-locked operation in Nd:KGW with hot-band diode pumping. Our results open the way for further power scaling of ultrashort pulse Nd:KGW lasers.

1.4 Contributions

The results of this work were presented at the Photonics North 2016 conference as a poster presentation. This article is available here [26]. Later, digest of whole experiment, some background information and final results of the laser system were reported in a peer-reviewed scientific journal Laser Physics Letters which is published by Institute of Physics (IOP) in United Kingdom. The article is published and available for viewing online here [27].

1.5 Outline

In this work, we demonstrated passive mode-locking of a Nd:KGW laser, generating 2.4 ps long pulses at a repetition rate of 83.8 MHz. To investigate pump absorption and reduce thermal effects, the crystal was pumped at 910 nm. The average output was measured to be 87

mW at 1067 laser emission. For mode-locking purpose, a SESAM was incorporated as an end mirror in the cavity.

In Chapter 2 background information about the neodymium ion and KGW crystal are discussed. Listed physical and optical properties of the crystal will justify the reasons behind choosing the N_g-axis cut Nd:KGW as active medium. Previous experimental work done using this crystal under diode-pumping in different regimes is covered afterwards. This chapter is concluded with a summary of recent trend of ~ 900 nm diode-pumping in Nd-doped crystals and applicability of the idea to the Nd:KGW.

Chapter 3 provides a brief idea about the mode-locked laser oscillator. Passive mode-locking theory with fast saturable absorber is provided for the convenience of general readers. Later, experimental design and set up of the laser system is explained.

Results and discussions are presented in 3.2.2. Reduction of quantum defect due to the longer pumping wavelength, CW regime results and thermal lensing power in the active medium are included along with the pulsed regime results. Finally, summary and intended feasible future work are mentioned in 0.

Chapter 2 Properties of Nd:KGW

The gain medium Nd:KGW is introduced in this chapter. A glimpse of neodymium ion and KGW crystal properties is provided in the beginning. Physical, mechanical and optical properties of Nd:KGW are reported in the following sections. Effect of doping concentration is also discussed in brief. Distinguishable previous works accomplished based on this crystal are listed in the previous works section. For the sake of simplicity this discussion is limited to only laser diode pumped system, also known as '*Diode-pumped solid-state laser'*- DPSSL.

2.1 Review of Nd:KGW

Nd:KGW is a promising active medium for low-to-medium range output power. Key features of this crystal are:

- *Low Threshold:* starts lasing at low pump power
- *Raman Converter:* KGW acts as Raman active media
- *Bandwidth (FWHM):* Larger bandwidth of the Nd:KGW emission (720 GHz) relative to YAG (120 GHz) is helpful to generate ultrashort pulses [28]

It is a four level laser system at 1067 nm. So far the common trend is to pump Nd:KGW at ~810 nm and achieve lasing at 1067 nm.

2.1.1 Neodymium ion

Neodymium (Nd) is one of the rare earth elements and atomic number is 60. In periodic table this element is placed inside the trivalent Lanthanide group which appears at the bottom. It was never found in nature as a free element but in the form of compounds e.g. monazite or bastnaesite. Main applications of this element are to make strong magnets ($Nd_2Fe_{14}B$) and Nd-doped lasers. The electron configuration of this element is [Xe] $6s^2$ $4f^4$. Five stable isotopes are found in nature among which ^{142}Nd is the most abundant. When neodymium is introduced

inside any host material, energy levels are split into vibrational manifolds via Stark effect and required electron transitions for lasing action take place inside the Nd^{3+} ion. There is a wide variety of materials which can act as a host for Nd^{3+} ion and result in broad emission bandwidths around 1060 nm suitable for ultrashort pulse generation e.g. Nd:glass, Nd:KGW, Nd:YVO_4, Nd:YLF and Nd:YAG [29, 30, 31, 13]. Often Nd doping is used in fibers to achieve high power fiber laser with good beam quality [32]. In addition, frequency doubling of the infrared fundamental radiation of the Nd-ion provides direct route to obtain visible laser radiation suitable for pumping of other important gain media such as Ti:sapphire [33] and Alexandrite [34].

2.1.2 KGW Crystal

To achieve desirable lasing action it is a must to select such a host material which has excellent optical, mechanical and thermal properties to withstand high intracavity power and act as a potential gain medium. Besides, host material has to incorporate small amount of doping elements without significant distortion. Despite being expensive to fabricate crystalline hosts, they offer decent thermal conductivity, large emission and absorption cross-sections and relatively broad emission bandwidth. KGW crystals have larger gain bandwidth compared to other crystals. For example, Nd:KGW has a large gain bandwidth of ~2.73 nm compared to Nd:YAG (0.6 nm) or Nd:YLF (1.3 nm). This crystal also offers fairly high stimulated emission cross-section, which is important for passive mode-locking and avoiding Q-switching instabilities. At low pump energy (0.5 – 1J), efficiency of Nd:KGW laser is 3 – 5 times higher than efficiency of Nd:YAG one [35].

2.1.3 Physical properties of KGW

KGW crystallizes from the melt in tetragonal symmetry and at around 1075 ^{0}C it undergoes a polymorphic transition to a monoclinic lattice. This biaxial monoclinic structure

is responsible for being anisotropic in its mechanical and optophysical properties. It belongs to space group C^6_{2h}. In Table 2.1 the unit cell parameters of KGW are summarized [23].

Table 2.1 Parameters of the unit cells and density of Gd^{3+} ions in $KGd(WO_4)_2$

a (A)	*b* (A)	*c* (A)	*β* (deg)	Volume of unit cell (V A^3)	Molecular weight (a.u.)	Density of Gd^{3+} N x10^{22} cm^3
8.098	10.417	7.583	94.43	637.8	692	0.627

In the KGW crystal the optical indicatrix axes N_m and N_g do not exactly coincide with the crystallographic axes as shown in figure 2.1 [23]. Here [010] crystallographic axis matches with the N_p optical indicatrix, but the N_m and N_g differ from the [100] and [001] directions by ~24^0 and ~20^0, respectively.

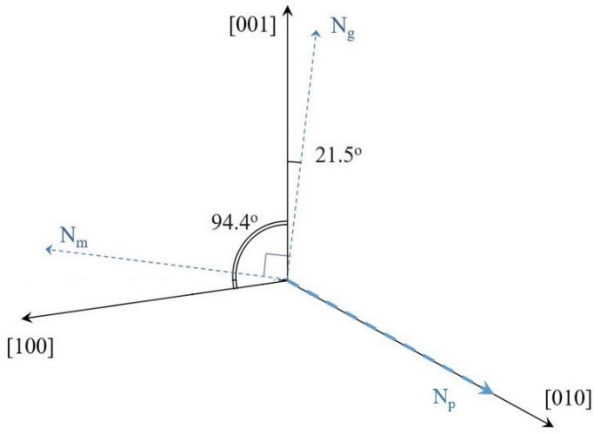

Figure 2.1: Mutual orientation of the crystallographic axes and the optical indicatrix in KGW crystal.

This crystal has fair mechanical hardness and fracture strength as listed in Table 2.2 [23]. As stated before, thermal conductivity of Nd:KGW is poor compared to other crystals, it is somewhat in between the Nd:YVO and Nd:glass. Thermal expansion factor results in end face bulging i.e. thermal lensing. This effect prevents Nd:KGW to be operated at high power.

Yumashev *et al.* reported that the combined thermo-optic effect and stress induced refractive index variation within Nd:KGW lead to the generation of an astigmatic thermal lens [16].

2.1.4 Optical properties of KGW crystal

Main optical & thermo-optical properties of this crystal are listed in Table 2.3.

Table 2.2 Mechanical and thermo-physical parameters of KGW

Property	Unit	Value along [100]	Value along [010]	Value along [001]
Knoop micro hardness	H (kg/mm^2)	370	390	460
Ultimate strength	σ (kg/mm^2)	14	10.2	6.4
Young's modulus	E (GPa)	115.8	152.5	92.4
Thermal expansion coefficient	γ [x 10^{-6} K^{-1} (for 100 ^{0}C)]	4	1.6	8.5
Thermal conductivity	λ [Wm^{-1} K^{-1} (for 100 ^{0}C)]	2.6	3.8	3.4
Density	gcm^{-3}	7.248 (doping 3 at.%)		
Specific heat	$JKg^{-1}K^{-1}$	500		

Table 2.3 Optical and thermo-optical properties of KGW

Refractive index @ 1.067 μm	η_p= 1.937 [E//Np] η_g= 2.033 [E//Ng] η_m= 1.937 [E//Nm] [23]	
Fluorescence lifetime	120 μs [dependent on Nd concentration] [35]	
Stimulated emission cross section	3.3×10^{-19} cm^2 at 1067 nm 0.76×10^{-19} cm^2 at 1350 nm [35]	
Lasing lines	910, 1067 and 1350 nm	
Absorption lines	810, 880 and 910 nm	
Temperature coefficient of refractive index dn/dT x 10^{-6} K^{-1} [36]	$k//N_p$	-15.47
	$k//N_g$	-13.70
	$k//N_m$	-18.06

The Nd:KGW crystal used in this experiment was procured from Altechna. Specific information acquired about this crystal from the product specification chart is listed in table 2.4.

Table 2.4: Nd:KGW crystal specifications (Altechna)

Doping Concentration	3%
Dimensions	1.6x6x20 mm
Geometry	flat/flat
Coatings	AR/AR (R<0.25%) @ (1067+1350 nm) AR/AR (R<5%) @ (810 nm)
Length tolerance	±0.1 mm
Dimensional tolerances	+0/-0.05 mm
Surface quality	10-5 S-D
Surface flatness	<λ/10 @ 632.8 nm
Parallelism error	<10 arcsec
Perpendicularity	<10 arcmin
Protective chamfers	<0.1 mm x 45°

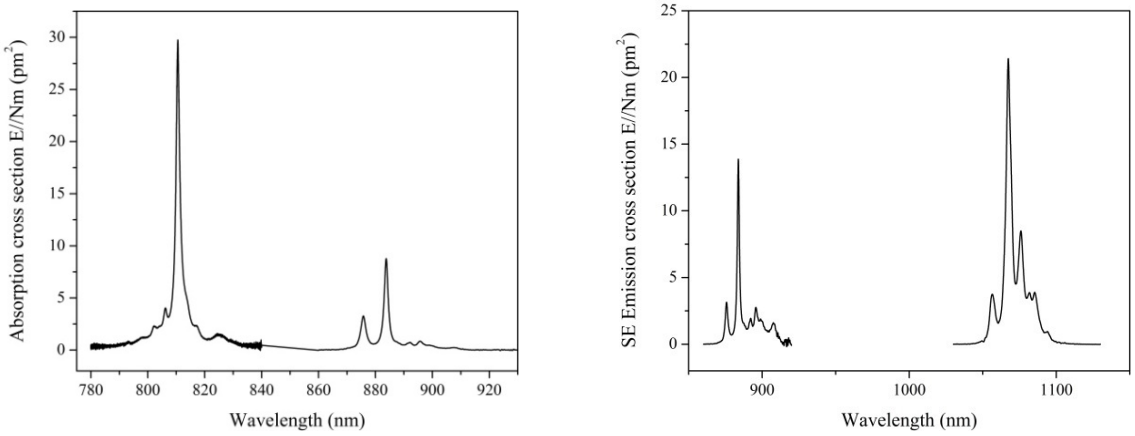

Figure 2.2: Absorption and emission spectra of Nd:KGWfor the E//N_m polarized light [37]. Image reproduced with permission.

In figure 2.2 absorption and emission spectra are provided for T = 300 K and E//N_m polarized light which has the strongest gain [37]. Although less common, other lasing polarizations can be also used in cases where lower gain is needed. For example in Q-switched

lasers this enhances energy storage in the crystal and can provide generation of more energetic pulses.

2.1.5 Effect of doping concentration

Level of doping concentration of active ions inside the host material has significant effects on the resultant optical and physical properties. In case of Nd:YAG, Nd:YLF or Nd:YVO_4, Nd^{3+} active ions substitute Y^{3+} ion. Ionic radius of Nd^{3+} is 1.12 Å which is different from ionic radius of Y^{3+} of 1.05 Å, resulting in high local host distortion that degrades crystal quality. The ionic mismatch is largely reduced in Nd:KGW, where Nd^{3+} substitutes Gd^{3+} of ionic radius 1.06 Å [38]. Thus for Nd:KGW doping concentration up to ~8% is achievable without significant host distortion. High level of doping is beneficial for development of micro-chips lasers [39, 40], where crystal length is often as short as 0.5 mm and strong pump absorption is needed.

2.2 Previous works on Nd:KGW

First lasing operation in double tungstate was explored in flashlamp pumping by Kaminskii *et al.* [18] where the crystal was Ln^{3+} doped. In nineties flashlamps were very popular to pump bulk laser crystals. In flashlamp-pumped systems, some reports establish the fact that Nd:KGW offers higher efficiency and lower threshold compared to Nd:YAG – most popular laser crystal at that time [41, 42]. Nowadays flashlamps are replaced by laser diodes and most of the solid-state laser systems are based on DPSSL technique. Reference [43] is believed to be the first demonstration of CW lasing in Nd:KGW with diode pumping.

2.2.1 Raman Scattering

Raman scattering is an inelastic light scattering phenomenon. When laser beam interacts with the gain medium, most of it is transmitted and part of it is scattered. Due to antireflection

coating, probability of reflection at lasing wavelength is very small. Over ~90% of the scattered radiation has the same frequency as the incident beam but a small portion of it has frequencies different from that of the incident beam. It utilizes the nonlinear optical response of the gain medium in intense radiation fields to generate additional spectral output lines. The strongest interaction is for the output shifted towards a longer wavelength (first Stokes shift), but at sufficiently high pump intensities additional lines at longer, as well as shorter wavelengths with respect to the lasing wavelength will appear (Stokes and anti-Stokes lines). By equipping highly reflective mirrors at these wavelengths in the cavity, moderate output power can be achieved through the output coupler.

Tungstate crystals are proven to have efficient lasing when doped with rare earth materials. These crystals also have large third-order nonlinear optical susceptibility (χ^3) for efficient stimulated Raman scattering (SRS). Combining these two features, the tungstate crystals are capable of being used as '*self-stimulated Raman lasers'* to convert laser emission wavelength to a specific wavelength for enriching the spectroscopic abilities of solid-state lasers [44]. A comparison of key spectral properties of well-known laser crystals is listed in table 2.5.

Being anisotropic, KGW features strong Raman transitions along two crystal axes, 901 cm^{-1} shift being dominant along the N_m-axis and 768 cm^{-1} along the N_g-axis (compared to a single strong transition in YVO_4 and $GdVO_4$), and so has potential for enhanced wavelength versatility [45]. Nd:KGW can also support both laser and Raman generation simultaneously as was mentioned above. Combination of '*laser gain medium*' and '*Raman process*' into one single element results in reduced number of cavity optical surfaces, thus minimizing the intracavity loss. Raman conversion in Nd:KGW was successfully accomplished in pulsed domain, but realizing Raman conversion in CW regime still remains challenging. The first

demonstration of CW self-Raman laser was done in [46]. A demonstration of CW self-Raman lasers with different Raman shifts of the Nd:KGW crystal at 1077.9 nm (89 cm^{-1}), 1162.9 nm (768 cm^{-1}), 1181.2 nm (901 cm^{-1}), and 1193.7 nm (89cm^{-1} + 901cm^{-1}) was reported by Tang *et.al* [47]. In table 2.5 a comparison of spectral properties among popular Raman crystals are listed:

Table 2.5: Key spectral properties of selected Raman crystals [48]

Crystal	Raman Shift	Raman linewidth	Integrated cross-sec	Raman Gain g_L @ 1064 nm	Raman Gain g_L @ 532 nm	Damage threshold
	cm^{-1}	cm^{-1}	(arb. units)	cm/GW	cm/GW	GW/cm^2
KGW	768 901	6.4 5.4	59 54	4.4 3.5	11.8	~10
KYW	767 905	8.4 7	65 50	3.6 5.1	21	
$GdVO_4$	885	3.0	92	> 4.5		~1
YVO_4	892	2.6	92	> 4.5		~1

The Stokes and anti-Stokes radiation of stimulated Raman scattering at 1181 nm and 973 nm was generated as a result of self-frequency conversion of the 1067 nm Q-switched Nd:KGW laser radiation in [49].

Owing to the relatively high emission cross-section at 1350 nm along with high Raman gain coefficient [18] this crystal is attractive as Raman converter to realize eye-safe spectral range at 1540 nm. Major *et al.* reported pulsed generation at eye safe range of ~1537 nm by focusing intense picosecond laser pulses around 1350 nm on KGW with conversion efficiency of 10% and reported Raman gain coefficient of ~0.8 cm/GW [21].

In self-Raman lasers thermal load is deposited in the gain medium from the following main sources:

- Inelastic nature of the Raman shifting process, which generates phonons during the wavelength conversion;
- Quantum defect, difference between the pump photon and energy photon;
- Non-radiative pump absorption, absorbed pump does not convert to laser.

Since KGW crystal suffers from poor thermal conductivity, for high power Raman generation this crystal is often used as a Raman shifter while another laser crystal seeds at fundamental wavelength. The high power output comes at the cost of higher resonator losses, because there are more crystal interfaces, and they are not as compact as the self-Raman laser [50]. Aiming at generating high power output, in some experiments KGW crystal converts the fundamental wavelength radiated by another gain medium in the resonator. A KGW crystal was used inside the Nd:YLF laser cavity as a Raman shifter producing 6.1 W at output wavelengths between 1140-1155 nm [51]. The output emission linewidth of pulsed KGW Raman laser is quite large and steps towards linewidth narrowing were demonstrated by Savitski *et al.* in [52].

All of the mentioned works in this section were accomplished with ~810 nm laser diode pumping. Recently there was a report on 880 nm fiber-coupled laser diode pumping achieving fundamental output power of 7 W from a two mirror cavity and 283 mW of maximum Stokes power at 1181 nm [45] in CW operation.

It is worth noting that Yb-ion doped KGW (Yb:KGW) also works efficiently as self-Raman laser. Based on a shorter Raman shift of 89 cm^{-1}, diode-to-Stokes optical conversion efficiency as high as 21.8% was achieved in Yb:KGW. This high efficiency results from the

small quantum defect because of diode pumping at 981 nm and high quantum efficiency of the smaller Raman shift [53].

The KGW crystal was also demonstrated to compress Stokes pulse width with respect to the pump laser pulse by backward stimulated Raman scattering [54].

2.2.2 Q-switched Regime

Q-switched lasers are popular for cutting and drilling. Passively Q-switched operation with Nd:KGW was demonstrated by Grabtchikov *et al.* under diode pumping where V:YAG was used as saturable absorber resulting in 78 ns pulses at an average output power of 87 mW [55]. Pumping this crystal at ~810 nm has limited its maximum average output power to 234 mW [56] and single pulse energy to 12 μJ [57] because of poor thermal and mechanical characteristics. Recently Huang *et al.* demonstrated Q-switched Nd:KGW laser with average output power as high as ~1.6 W under 877 nm pumping [12] owing to the reduced effects of thermal lensing.

2.2.3 Mode-locked Regime

Mode-locked lasers provide short and intense pulses of light which have been extensively used in industry and academia. First CW mode-locked operation of Nd:KGW laser under diode-pumping was demonstrated by Flood *et al.*, producing 12 ps pulses with the help of Brewster-angled lithium-niobate electro-optic phase modulator [58]. The autocorrelation trace of output pulse showed wings on the pulse; which was interpreted as possible indication of satellite pulse. Similar output was observed for mode-locking with strong Spatial Hole Burning (SHB) [59]. Kerr-lens mode-locking in a flash-lamp pumped crystal was demonstrated by M. Lettenberger *et al.* generating around 1.7 ps short pulses [60]. Passive mode-locking under 808 nm diode-pumping was demonstrated by A. Major *et al*. utilizing saturable Bragg reflector and producing 6.3 ps pulses with 1 W of average power [13]. Before saturable

absorber mirrors or quantum wells has been fully developed, additive pulse mode-locking (APM) was one of the popular mode-locking methods. The pulse formation in an APM mode-locked laser is based on the coherent superposition of a pulse in the main cavity and a pulse from the coupled cavity that have experienced a nonlinear phase shift, i.e. self-phase modulation in an optical fiber, leading to constructive interference at the peak of the pulse and destructive interference in the wings. Till this date, the shortest pulse duration under diode pumping from the Nd:KGW was recorded to be 1.9 ps by exploring the APM technique. Up to 0.85 W of output power was achieved with 2.3 ps pulse duration at a repletion rate of 76.5 MHz [14].

It is interesting to note that mode-locking of KGW crystals doped with Yb-ions was also demonstrated [61, 62, 63, 64] producing pulses in the femtosecond regime.

2.3 Motivation for longer wavelength pumping

Some Nd-doped solid-state crystals were pumped at longer aiming at reducing quantum defect thus improving efficiency and stability of lasing operation. Pumping directly to emitting laser level improves efficiency and stability of the system.

2.3.1 Nd-doped crystals diode pumped at ~910 nm

In recent works it has been demonstrated that pumping of Nd-doped crystals at >810 nm results in better performance with excellent pump absorbance. Lupei *et al.* proposed a novel pumping scheme for Nd:YVO_4 laser which had achieved slope efficiency as high as 80% [65]. The idea was to increase the ratio between the pump and lasing wavelengths as mentioned in equation 2.1, i.e. to decrease the quantum defect (QD).

$$P_{out}(T) \approx \frac{T}{T + L_i} \frac{\lambda_P}{\lambda_L} \eta_a (P_{P,inc} - P_{th}) \tag{2.1}$$

where P_{out} is the average output power through the output coupler, T is transmission of the output coupler, L_i is losses inside the cavity, $P_{P,inc}$ and P_{th} are the incident pump and threshold pump power, λ_P and λ_L are pump and laser wavelength and η_a indicates ratio between pump and laser beam waist, which is typically valued 1 for four-level system [66]. In general for Nd-doped crystals, pump radiation at ~810 nm is strongly absorbed, but electrons are pumped to $^4F_{5/2}$ level, which introduces a parasitic upper QD between the pumping and emitting-laser level (see figure 2.3). Keeping laser emission fixed at 1-μm range, this upper QD could be eliminated by pumping at ~880 nm directly into the emitting-laser level $^4F_{3/2}$ as shown in figure 2.3.

Slope efficiency can be defined as slope of the curve which is acquired by plotting output power versus pump power. Theoretically, the slope efficiency of Nd:YVO_4 at 1064-nm laser emission for 809 nm and 880 nm diode-pumping would be 76% and 82.7%, respectively because in 880 nm pumping the ratio of the pump to laser wavelength is increased, i.e. the QD is reduced. Pumping the crystal directly into the $^4F_{3/2}$ was reported by Sato *et al.* as well [65].

Later Sangla *et al.* pumped Nd:YVO_4 at 914 nm, which achieved 11.5 W of output power at 1064 nm. Instead of pumping from the ground manifold level Z1, in that work electrons were pumped from thermally populated highest sub-level Z5 of the ground state manifold. In this way, theoretically slope efficiency of 85.9% is achievable. In this experiment the slope efficiency of 80.7% and optical-to-optical efficiency of 78.7% was achieved [67] which are the highest reported for Nd:YVO_4 till this date. In mode-locked regime the highest reported to date slope efficiency was 77% [68].

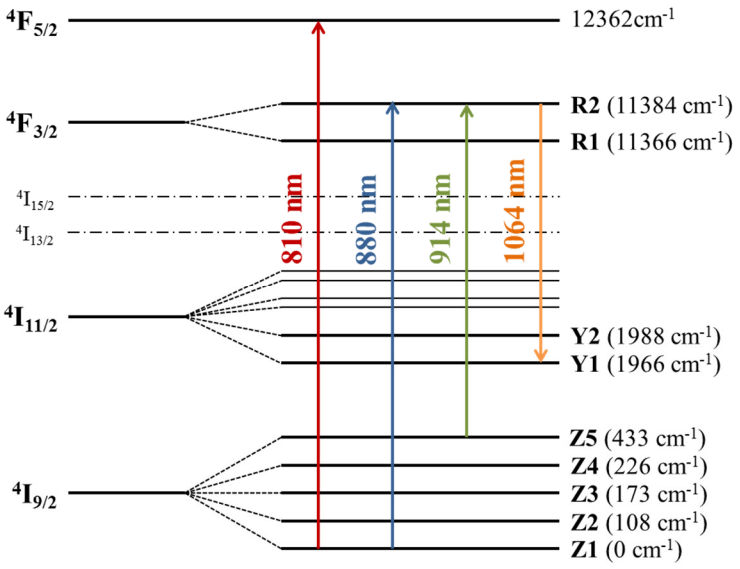

Figure 2.3: Energy level diagram of Nd:YVO_4.

Utilizing a similar tactic, Nd:$GdVO_4$ was diode-pumped at 913 nm. Using 8 W laser diode, 4.3 W was absorbed, which translates to ~53.8% of pump absorption. The maximum average output power was 3.32 W in the CW regime, corresponding to 77.2% and 81.2% of optical conversion efficiency and slope efficiency, respectively [69]. Energy level diagram of Nd:GVO is shown in figure 2.4.

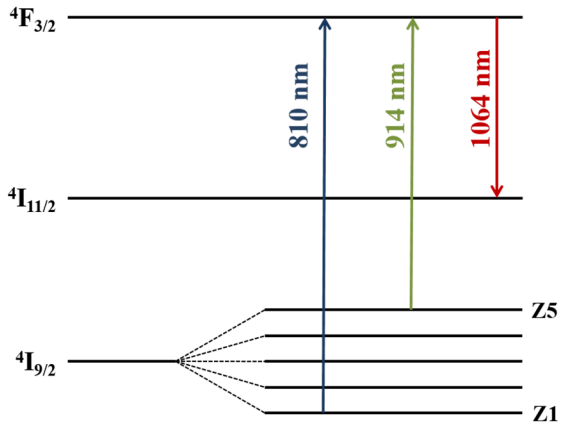

Figure 2.4: Energy level diagram of Nd:$GdVO_4$ [69].

For Nd:KYW, a sister material of Nd:KGW, the crystalline splitting of energy states scheme of Nd^{3+} ions at 77 K is reproduced from [70] in figure 2.5. The $^4F_{5/2}$ level is excluded

in the figure since it corresponds to ~810 nm pump. Lasing was observed at 913.7 nm and 1354.4 nm and transition cross-sections were reported to be 0.1×10^{-19} cm^2 and 4.3×10^{-19} cm^2 respectively. In the literature there are no record of utilizing 913 nm lasing line to pump the Nd:KYW crystal.

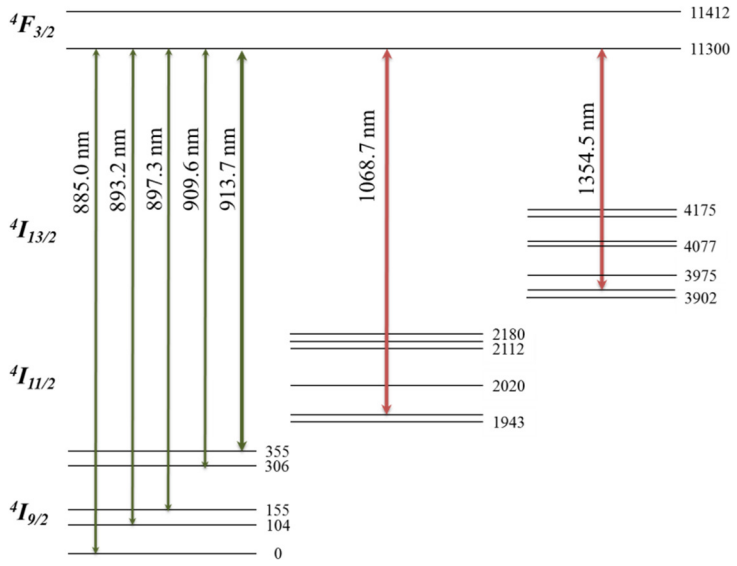

Figure 2.5: Energy level diagram in Nd:KYW. The positions of the levels are given in inverse centimeters. Observed lasing lines are indicated by thick lines.

The same idea was applied to Nd:YAG, another excellent crystal, by experimenting with diode pumping at 885 nm. This resulted in little increase in slope efficiency from 49% for 808 nm pumping to 54% for 885 nm due to the low pump absorption [71].

2.3.2 Motivation for ~910 nm pumping in Nd:KGW

The emission spectra of Nd:KGW in the 860-940 nm wavelength range are shown in figure 2.6 and were acquired from a 1.9 mm thick 3 at.% Nd:KGW crystal [17]. In the fluroscence spectrum, there is a small bump at ~910 nm. This transition can be used for fluorescence as well as absorption because of thermal population of Z5. If a laser diode pumps a longer crystal at this wavelength, a fair amount of pump can be absorbed in the crystal. In our work this specific lasing line at 910 nm was used for diode pumping.

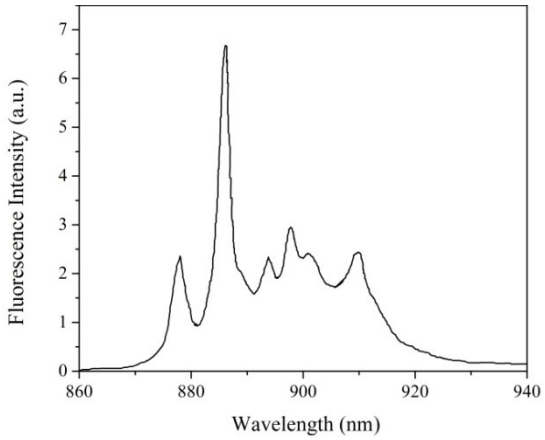

Figure 2.6: Emission spectra of Nd:KGW in the >860 nm range [17].

Recently there were several reports on pumping of Nd:KGW crystal at longer wavelengths. Bui *et al.* pumped the N_g-cut and N_p-cut Nd:KGW at 879 nm with 17.3 W and 26.8 W pump power, respectively, before thermo-mechanical damage took place and resulted in 5.4 W and 9.4 W of output power in CW regime. A simple two mirror cavity was employed. Differential lasing (i.e. slope) efficiency for the N_p-cut laser was reported ~66% with respect to the absorbed pump power [25]. A maximum fundamental output power of 7.0 W was achieved with 27 W of incident pump power in [45]. Pumping at ~880 nm shows promises of good results in the literature which keeps the way open for investigation of further quantum defect reduction by pumping wavelengths longer than ~880 nm.

Better laser performance in Nd:YVO_4 and Nd:$GdVO_4$ was demonstrated with long wavelength >910 nm diode pumping. Quantum defect reduction helps to reduce the effect of thermal lensing. With 914 nm pumping, thermal lensing in Nd:YVO_4 can be reduced by a factor of two [72]. Since Nd:KGW suffers from poor thermal conductivity, to optimize for higher output power and lower thermal lensing, in our experiment it was pumped at 910 nm using a fiber-coupled laser diode.

Chapter 3 Experimental Theory & Design

A brief overview of general CW operation of DPSSL is given in the beginning of this chapter. Later, a comprehensive discussion on passive mode-locking theory is provided for better understanding of the following experimental design section. In the experimental setup part all components and their performance are studied rigorously.

3.1 Passive mode-locking theory

This section starts with an overview of basic lasing operation. The three principal elements leading to gain in a solid-state laser are as follows [15]:

- The host material with its macroscopic mechanical, thermal, and optical properties.
- The activator/sensitizer ions with their distinctive charge states.
- The optical pump source with its particular geometry and spectral irradiance.

In the activator/sensitizer three fundamental processes e.g. absorption of pump, spontaneous emission at random wavelength and stimulated emission take place. Pumping source produces population inversion inside the gain medium, meaning that a higher number of electrons stay in the excited energy state as compared to the number of electrons in the lower laser state. However stable CW lasing is not possible without the positive feedback from the optical resonator.

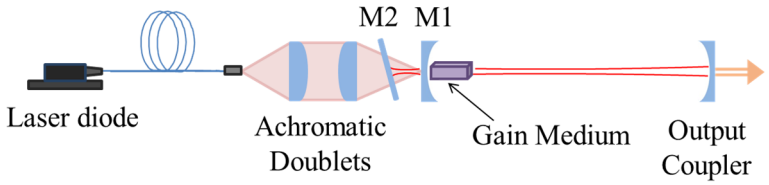

Figure 3.1: Diode pumped Fabry-Perot-type solid-state laser.

The gain medium coherently amplifies light passing through it. In order to start lasing, the gain medium has to be excited with threshold pump power (P_{th}). To achieve P_{th}, roundtrip gain has to compensate for roundtrip loss as shown in equation 3.1,

$$G = R_1 R_2 e^{2(g-\alpha)L} \tag{3.1}$$

where, G = roundtrip gain (provided by gain medium), R_1, R_2 = reflectivity of mirror M1 and output coupler, respectively, g = effective gain coefficient, α = effective loss coefficient and L = cavity length. At threshold, $G_{th} = 1$ and equation 3.1 can be reduced to

$$2gl = -\ln R_1 R_2 + 2\alpha L \tag{3.2}$$

Mirror M1 is a highly reflective so leakage will be very low. Output coupler has some transmission. These two losses are compensated by the gain medium so that at threshold the roundtrip gain becomes equal to the roundtrip loss. Above threshold pump power, some portion of emission is released through the output coupler. Gain bandwidth of the active material and optical properties of Fabry–Perot-type resonator (as shown in figure 3.1) determine the spectral output from the laser. The transverse mode of laser beam is usually TEM_{00} (i.e. fundamental Gaussian mode). In normal condition many resonance peaks of the resonator lie within the spectral width of the laser material leading to many oscillating longitudinal frequency modes. The radiation spectrum emitted from a laser therefore consists from a number of discrete wavelengths (i.e. longitudinal modes) [15].

In frequency domain, the basic laser operation is illustrated in figure 3.2. The bell-shape laser gain is provided by the gain medium which works as a bandpass filter. Cavity loss is assumed to be frequency independent and indicated by a dashed horizontal line. Laser oscillation occurs only at those frequencies where the gain line exceeds the loss. For this reason multiple frequencies (or wavelengths) appear at the output simultaneously which causes homogenous broadening of the output spectrum. These modes are spaced at frequency of

$$\Delta f = \frac{c}{2L} \tag{3.3}$$

where Δf represents mode spacing.

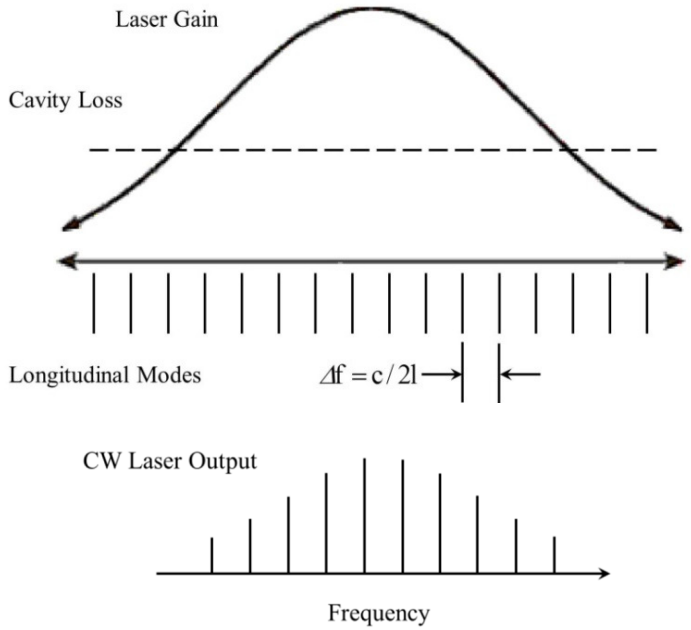

Figure 3.2: Gain and loss spectra, longitudinal mode locations, and output of a homogeneously broadened laser under single-mode operation [73].

3.1.1 Principles of mode-locking

In a free-running laser, both longitudinal and transverse modes oscillate simultaneously without fixed mode-to-mode amplitude and phase relationships. The resulting laser output is a time-averaged statistical mean value [15]. In mode-locking technique, all of the longitudinal modes are forced to interfere constructively so that strong and intense pulses of light can be generated. To have constructive interference, coherent phase relationship between the multiple modes is a must. In figure 3.3 generation of light pulse from a constructive interference of six longitudinal modes is presented. This is achieved by introducing a periodic loss modulation inside the cavity.

Indication of first mode-locking appears in the work of Gurs and Muller [74, 75] on ruby lasers. At the same time period Statz and Tang reported mode-locking in He-Ne laser [76]. The analytic theory including closed-form analysis of active and passive mode-locking with slow and fast saturable absorber was developed by Hermann A. Haus [77].

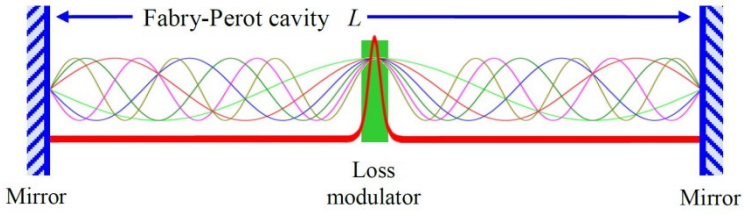

Figure 3.3: Schematic longitudinal illustration of the pulse formation in a Fabry-Perot cavity with six modes locked in phase [78].

3.1.2 Types of mode-locking

The two main types are active and passive mode-locking. In active mode-locking, induced signal for loss modulation in the cavity is provided externally, while in passive mode-locking it is done intrinsically by placing special element (absorber) inside the cavity. Utilizing acousto-optic, electro-optic or a Mach–Zehnder integrated optical modulator, active mode-locking is achieved when the modulation is synchronized with the resonator roundtrip time. These loss modulators are electronically externally driven and produce sinusoidal weak loss modulation as shown in figure 3.4. From the time domain, at the minimum of loss modulation net gain exceeds the loss, thus a short pulse is formed. This means that the modulator acts like a periodic shutter which opens once per pulse roundtrip time. In the frequency domain, modulation of a fundamental laser mode (which is favored by gain bandwidth of active material) by the external signal creates sidebands with the same phase relationship. These sidebands couple to adjacent cavity modes and so on. The longitudinal modes of the same phase relationship interfere constructively to generate a short pulse. Active mode-locking is disadvantageous due to external slow electronic driver and synchronization with roundtrip

time. For these reasons, ultrashort pulses in femtosecond range are not achievable in active mode-locking.

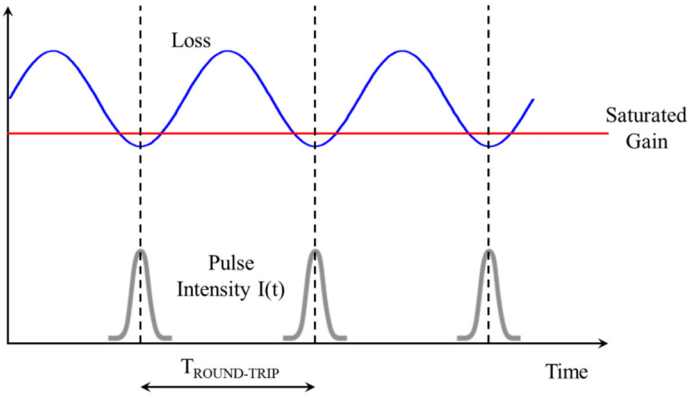

Figure 3.4: Active mode-locking in time domain.

Active medium has a limited gain bandwidth which also contributes to how short a pulse can be obtained. As a pulse travels through the laser cavity, frequency dependent phase variation takes place, which is known as dispersion. This effect broadens the pulse. In picosecond regime it is not a significant factor.

3.1.3 Passive mode-locking with fast saturable absorber

In order for the passive mode-locking process to start spontaneously from continuous wave operation, a nonlinear optical element is introduced into the cavity. In the CW regime, many longitudinal modes fluctuate altogether and the output is an average of them. The nonlinear element creates amplitude instability, meaning that intensive fluctuation or stronger noise will experience lower loss (and thus amplified), whereas less intensive parts face heavy loss and eventually are suppressed. The amplified intense fluctuation bleaches the absorption of the nonlinear element and thus grows in intensity. On the other hand, the wing parts of the intense fluctuation face strong absorption from the nonlinear element and hence are attenuated. This action takes form of a pulse. Successive passages of the high intensity radiation pulse

through the resonator result in a pulse train appearing at the output coupler. The pulse formation process over successive roundtrips is illustrated in figure 3.5.

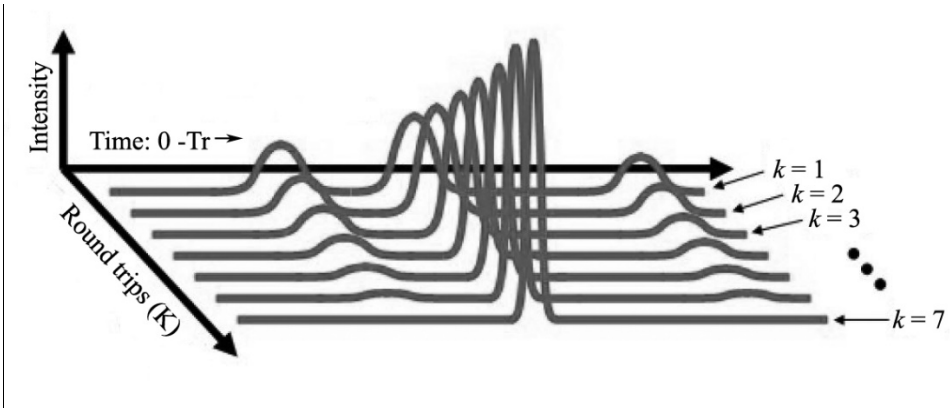

Figure 3.5: Initial high-intensity spike grows from roundtrip (k=1) to roundtrip (k=7) whereas other spikes are suppressed. At the same time pulse-shortening process takes place.

Passive mode-locking mechanisms are well explained by three fundamental models: slow saturable absorber mode-locking with dynamic gain saturation [figure 3.6(a)], fast saturable absorber mode-locking [figure 3.6(b)] and soliton mode-locking [figure 3.6(c)]. For solid-state lasers we can neglect slow saturable absorber mode-locking as shown in figure 3.6(a), because no significant dynamic gain saturation is taking place due to the long upper state lifetime of the laser [79]. The gain becomes saturated with the increasing lasing power and saturation of gain depends on pulse duration in case of dye lasers.

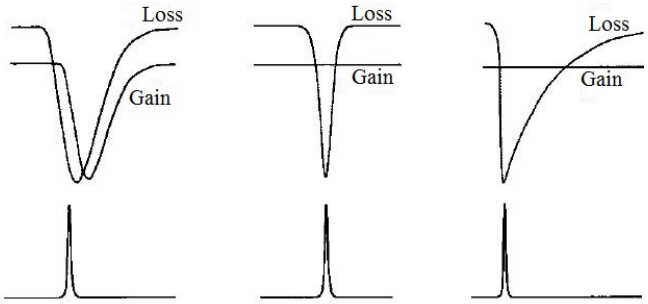

Figure 3.6: The three fundamental passive mode-locking models: (a) passive mode-locking with a slow saturable absorber and dynamic gain saturation, (b) fast absorber mode-locking (c) soliton mode-locking [79].

The dominant mode-locking mechanism is determined by the recovery time of the saturable absorber - which is either based on fast saturable absorber mode-locking in the positive or negative dispersion regime, or soliton mode-locking, which operates solely in the negative dispersion regime. This experiment was performed in positive dispersion regime by utilizing SESAM which had a recovery time of 1 ps and the generated pulse duration was 2.4 ps. SESAM comes with multiple advantages over other mode-locking techniques-

- SESAM mode-locked lasers can provide shorter pulse duration when compared with active mode-locking;
- Mode-locking is usually self-starting;
- Mode-locking with SESAM is comparatively less complex than Kerr lens mode-locking (KLM), because it imposes limitations on the cavity design and requires critical cavity alignment where mirrors and laser crystal have to be positioned to an accuracy of several hundred microns typically.

The description of mode-locking in terms of a pulse spectrum that evolves with time can be transformed into a description of a pulse with a temporal envelope that evolves on a time scale much longer than the pulse width. This is accomplished by a Fourier–transform with the Fourier–transform pairs

$$\left\{\begin{aligned} a(t) &= \int d\Omega \exp(j\Omega t) A(\Omega) \\ A(\Omega) &= \frac{1}{2\pi}\int dt \exp(-j\Omega t) a(t) \end{aligned}\right\} \tag{3.4}$$

where a(t) and A(Ω) are the complex amplitude of the pulse envelope circulating in the laser resonator in the time and frequency domain, respectively. From equation 3.4, pulse evolution equation was derived for active mode-locking [77] as per following:

$$\frac{1}{T_R}\frac{\partial}{\partial T}a(T,t) = (g-l)a(T,t) + g\left(\frac{1}{\Omega_g}\right)^2 \frac{\partial^2}{\partial t^2}a(T,t) - \frac{1}{2}M\Omega_m^2 t^2 a(T,t) \qquad (3.5)$$

where, T_R represents roundtrip time, T is a long term time variable when the pulse evolution is relatively slow, g & l are gain and loss, Ω_g is the gain bandwidth of laser crystal, M is modulation applied from external modulator and Ω_m is the modulation frequency, which is equal to frequency separation of successive modes.

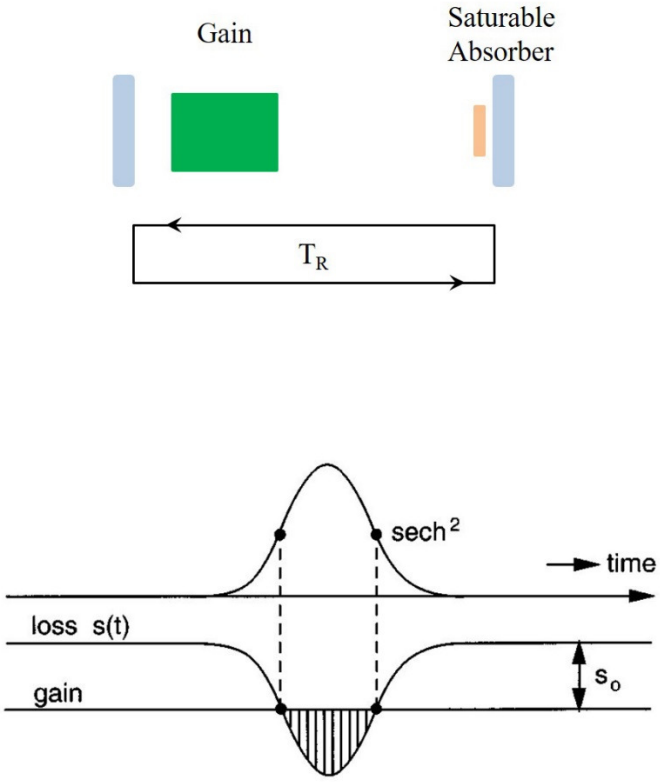

Figure 3.7: Dynamics of a laser mode-locked with a fast saturable absorber [77].

In passive mode-locking with fast saturable absorber, the loss modulation of the absorber s(t) in transmission through the absorber is,

$$s(t) = \frac{s_0}{1 + I(t)/I_{sat}} \qquad (3.6)$$

where s_0 (<1) is unsaturated loss, I(t) is dependent intensity and I_{sat} is the saturation intensity of the absorber. If the saturation is relatively weak, expression (3.6) can be expanded to give

$$s(t) = s_0 - {}^{s_0 I(t)}\!\!\diagup\!\!_{I_{sat}} \tag{3.7}$$

The intensity multiplied by the effective area of the mode gives the power in the mode. Normalizing the mode amplitude $|a(t)|^2$ represents the power. Then the transmission can be written,

$$s(t) = s_0 - \frac{s_0 |a(t)|^2}{I_{sat} A_{eff}} \equiv s_0 - \gamma |a(t)|^2 \tag{3.8}$$

where γ is the self-amplitude modulation (SAM) coefficient. To model active mode-locking in the steady state, the change of the pulse in one roundtrip is zero and then a closed form solution to differential equation is derived, which is mentioned in equation (3.5). The master equation of passive mode-locking with a fast saturable absorber is obtained by introducing the saturable loss into (3.5) and omitting the active modulation term. The unsaturated loss s_0 can be incorporated into the loss coefficient with the result

$$\frac{1}{T_R}\frac{\partial}{\partial T} a = (g - l)a + g\left(\frac{1}{\Omega_g}\right)^2 \frac{\partial^2}{\partial t^2} a - \gamma |a|^2 a \tag{3.9}$$

The solution is a simple hyperbolic secant,

$$a_0(t) = A_0 \operatorname{sech}({}^{t}\!\!\diagup\!\!_{\tau}) \tag{3.10}$$

with,

$$\frac{1}{\tau^2} = \frac{\gamma A_0^2 \Omega_g^2}{2g} \text{ and } 1 - g = \frac{g}{\Omega_g^2 \tau^2} \tag{3.11}$$

where τ is the pulse width. A few helpful conclusions can be derived from this equation (3.11). For example, it shows that the pulse width is inversely proportional to gain bandwidth

and SAM coefficient. The solution in (3.9) is not stable unless gain saturation is explicitly included. However, with SESAM there is no gain saturation in the cavity. Thus assuming an approximately constant gain during the passage of one pulse, equation (3.9) represents master equation of passive mode-locking with fast saturable absorber.

3.2 Experimental Design

Lasing operation takes place inside the laser cavity, which consists of a gain medium and multiple curved and plain mirrors as shown in figure 3.1. These mirrors and gain medium have special dielectric coating to allow reflection of specific wavelength and transmission of all other wavelengths. Gain medium compensates for the optical losses that take place inside the laser cavity. One of the end mirrors is called an output coupler, which is partially transmissive and allows a finite amount of laser light to couple out of the cavity. Unlike fiber lasers or waveguide lasers, there are no waveguide structures for solid-state bulk lasers, so the beam propagates in free space between optical components. Thus the beam radius in the gain medium is essentially determined not by the gain medium, but rather by the design of the laser resonator [80]. Dust particles or organic matters in the air may be deposited on laser mirrors and other components which reduces the overall efficiency in long term application. The mirrors and other optical components are usually attached to adjustable mounts on the optical table for better alignment and optimization.

While designing our laser cavity, we tried to satisfy multiple criteria such as minimized adverse effects of thermal lensing and aberrations in the gain medium, specific beam radius at SESAM and a good overlap between the pump and laser modes. As stated before, since one of the distinct features of Nd:KGW is that it has a lower threshold, the spot size at the laser crystal was maintained at 300 μm to ensure good mode matching. Based on these requirements we utilized ABCD ray transfer matrix analysis and reZonator software to specify which

components we were going to use, what would be the angle of incidence of each component and what are the distances between them.

Passive mode-locking in this cavity can be explained in simple words. In the CW regime output, there is always intracavity noise. One of the intense noise spikes saturates the absorption of SESAM. Due to absorption, electrons in SESAM quantum well jump to the excited energy state, losing capability of further absorbing the intense noise. Thus at high intensity everything is reflected and at low intensity everything is mostly absorbed by the SESAM and as a result a pulse is formed. This pulse circulates around the cavity and once it hits the output coupler, small portion of it is transmitted and major portion is reflected back to the cavity. Thus the self-amplitude modulation induced by SESAM results in a continuous wave mode-locked output. More details about the SESAM structure and operation can be found in section 3.2.2.4.

3.2.1 Laser Cavity Design

One of the important factors to achieve efficient lasing operation is to ensure a good overlap between the pump mode spot and the lasing mode spot at the gain medium. Other important factors such as stability and beam quality over a range of pump power, low sensitivity to alignment, minimizing roundtrip losses, required number of optical components and compactness are also considered.

3.2.1.1 ABCD Law

ABCD matrices were initially introduced to describe the propagation of rays. But this theory enables us to predict the parameters of a collimated Gaussian beam that exits from an optical system, provided that input Gaussian beam parameters and the ABCD matrix representing the optical system is defined beforehand. Utilizing this analysis, laser cavity can be designed and simulated to calculate precise distances between optical components. ABCD

matrix analysis can be used to design a cavity with the required spot sizes, and to verify the stability against changes in the length of the cavity arms.

The cavity in figure 3.8 was designed for this experiment where SESAM is used as one of the end mirrors and other curved mirrors (M1, M2 and M4) are replaced by equivalent lenses for the purpose of ABCD matrix analysis. A lens (FT) was considered inside the active material as an approximation of thermal lensing.

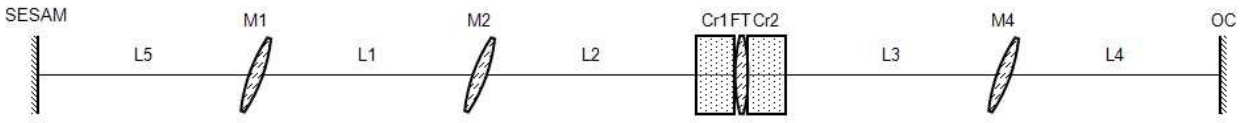

Figure 3.8: 5 mirror cavity for experiment.

3.2.1.2 Roundtrip matrix for designed system

Roundtrip matrix was found with reference to Cr1-FT interface (refer to figure 3.8) as per following:

$$M = Cr1 * L2 * M2 * L1 * M1 * L5 * SESAM * L5 * M1 * L1 * M2 * L2 * Cr1 * FT * Cr2 * L3 * M4 * L4 * OC * L4 * M4 * L3 * Cr2 * FT \quad (3.12)$$

In this cavity, transverse and longitudinal roundtrip matrixes are calculated to be as per following with reference point to crystal end-face; $P_T = -0.02$; $P_S = 0.067$.

$$M_T = \begin{bmatrix} -0.398 & 268.334 \\ -0.004 & 0.358 \end{bmatrix} \qquad M_S = \begin{bmatrix} -0.324 & 269.234 \\ -0.004 & 0.458 \end{bmatrix} \quad (3.13)$$

Intermode beat frequency of the system was 83.63 MHz and the total cavity length was = 1769 mm.

3.2.2 Experimental Setup

3.2.2.1 Pump Laser

The laser diode used in this experiment was procured from IPG Photonics. Center wavelength for this diode is 910 nm and the tolerance is ± 10 nm. The maximum output power

obtained from the diode was 16 W. This laser diode was attached to a fiber with ~105 μm core diameter with numerical aperture of 0.12.

Multiple advantages result from utilizing 910 nm laser diode instead of standard 810 nm one. First of all, due to recent developments in laser diode technology, it allows us to obtain commercially available 910 nm laser diodes at much cheaper cost as compared to the 810 nm ones. Beam quality from the 910 nm laser diode is at least 4 times better than from 810 nm one, which means even if we use a longer crystal there will be still better overlapping in between the pump and laser modes. Laser diodes at 910 nm have longer lifetime because they are built of InGaAs as compared to 810 nm laser diodes which are built of GaAlAs material.

The laser diode was water cooled at 16 ^{0}C to stabilize its output laser wavelength. We have observed a shift of operating wavelength due to the increasing diode temperature. Figure 3.9(a) shows the shift of wavelength with increasing of driving current when the laser diode was water cooled at 1300 CCM flow rate. By increasing the temperature of the diode, the band gap energy decreases and the emitted wavelength increases. It follows that the peak wavelength shifts to longer wavelength and therefore this shift is called the red shift.

The output of a laser diode was fiber coupled. The output spectrum of the laser diode at FWHM was ~5 nm wide as shown in figure 3.9(b). The pump imaging setup consisted of a collimating lens (CL, f = 40 mm) and a focusing lens (FL, f = 200 mm) to produce five times larger spot size in the middle of the crystal. The pump spot diameter in the crystal therefore was ~550 μm.

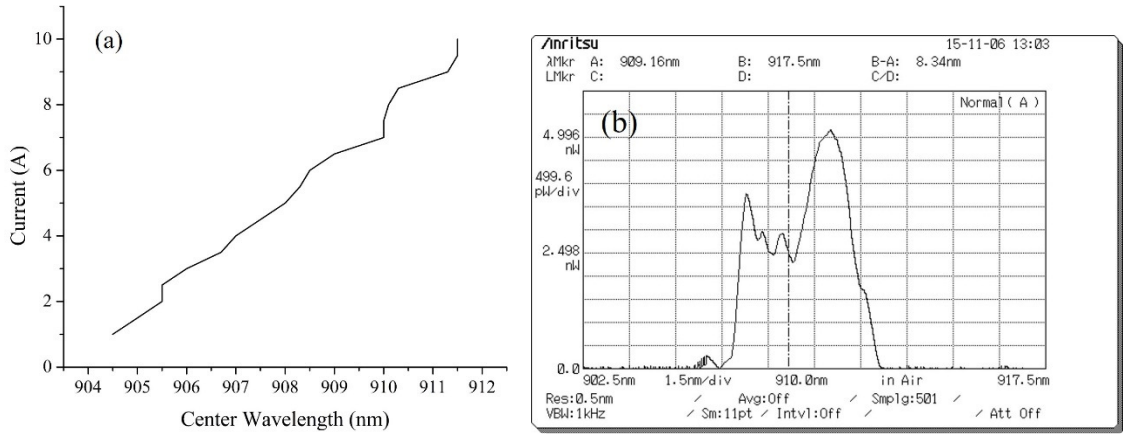

Figure 3.9: (a) Pump wavelength shift with increasing diode current; (b) Diode Spectrum at 8A drive current.

3.2.2.2 Laser Crystal

Laser crystal that was experimented with in this work is commercially available from Altechna. It was 20 mm long, N_g-cut Nd:KGW slab crystal with dimensions of 1.6x6x20 mm and 3 at.% doping concentration. Previous results show that the N_g-cut Nd:KGW allows one to obtain higher average output powers at high pump levels as compared to the N_p-cut Nd:KGW [81]. The thermal lens in the N_g-cut Nd: KGW was found to be weakly astigmatic with a positive refractive power for both the N_m- and N_p-directions. For the N_p-cut Nd:KGW, strong astigmatism was observed and the refractive powers in the N_g- and N_m-directions had opposing signs [82]. For these reasons the N_g-cut crystal was chosen over the N_m- and N_p-cut KGW. The crystal had flat end-faces which were antireflection coated at oscillating wavelength of 1067 nm. For better heat dissipation, the crystal was wrapped in indium foil and sandwiched in an aluminum heat sink. The crystal was also water-cooled at 16 ^{0}C.

3.2.2.3 Optical Resonator

A 5 mirror optical resonator was designed where lasing operation took place. In figure 3.10 the cavity components are discussed in brief. Components utilized in this experiment listed in table 3.1, where the last row shows distance in between components.

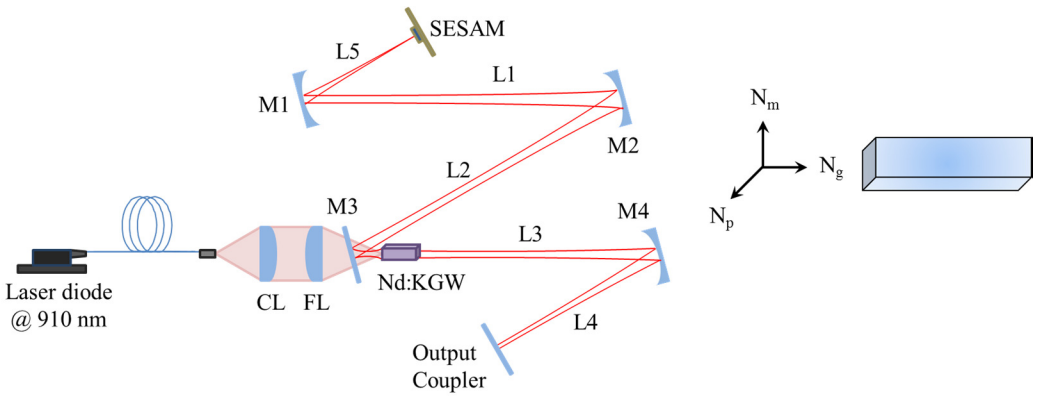

Figure 3.10: schematic of continuous wave mode-locked Nd:KGW laser. CL: collimating lens; FL: Focusing lens; M3: Dichroic mirror; M1, M2 and M4: concave mirrors with radii of curvatures 50, 400 and 500 mm respectively; SESAM: relaxation time ~1 ps, modulation depth ~6%. The inset indicates the orientation of the N_g-cut crystal with respect to laser propagation direction along the N_g axis. Crystal dimensions are 20 mm along the N_g-axis, 6 mm along the N_m-axis, 1.6 mm along the N_p-axis.

Table 3.1: Parameters used in equivalent lens waveguide of the designed cavity

Component	SESAM	Concave HR mirror (M1)	Concave HR mirror (M2)	Dichroic mirror (M3)	Nd:KGW Crystal	Concave HR mirror (M4)	Output Coupler
Properties (mm)		Radii = 50	Radii = 400		Length = 20	Radii = 500	Transmission = 1.6%
Distance (mm)		37	314	455	20	481	462

Figure 3.11 represents variation of the beam radius throughout the laser cavity. The smallest mode size is on the SESAM. The laser mode spot size at the crystal end-face was calculated to be ~600 µm (also see Appendix A). The pump imaging optics (achromatic doublets CL and FL) provided a 1:5 imaging setup and produced a ~550 µm pump spot size

diameter in the middle of the crystal. Considering pump divergence which had an M^2 of ~20, there was a good overlap between the pump mode and the laser mode.

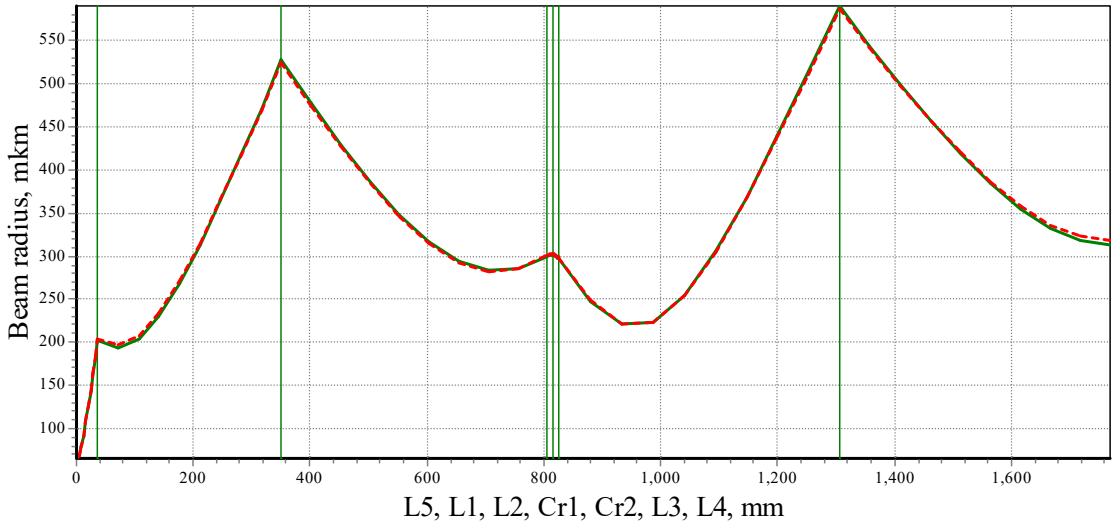

Figure 3.11: Laser beam radius variation inside the laser cavity.

Thermal lensing in solid-state laser can significantly affect lasing operation. Hot-band diode pumping at 910 nm reduces the amount of thermal heat deposited in the crystal. Owing to this advantage, high power pumping with the available diode was possible producing pump intensity of 3.6 kW/cm^2 in the crystal. . To evaluate the stability of the cavity against thermal lensing, a thin lens was introduced inside the crystal in the simulated cavity model to replicate thermal lensing effects. The following figure shows stability diagram of the designed cavity with respect to the focal length of the induced thermal lens. Stability condition developed in Appendix A defines the regions where the cavity is stable. The stable cavity must have the stability parameter in between -1 and +1. From figure 3.12, it is obvious that focal length of -50 mm to 125 mm corresponds to an unstable laser cavity.

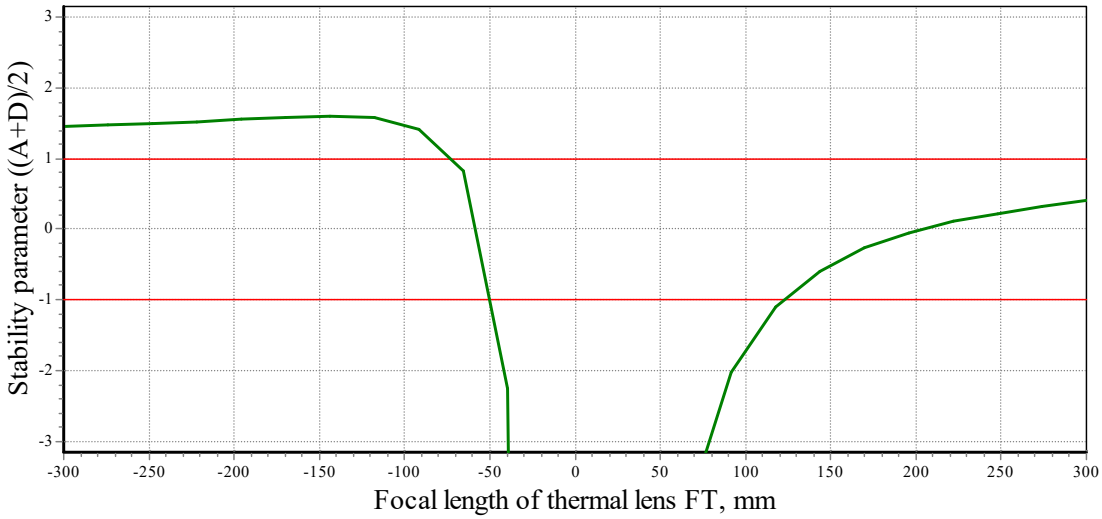

Figure 3.12: Stability diagram with respect to changes in focal length of the induced lens.

The variation of the beam radius at the output coupler (M4) with respect to the changes in the focal length of the induced thermal lens is shown in figure 3.13. According to the figure, both strong positive thermal lensing results in the increase of output mode radius at the output coupler which can lead to an unstable laser cavity.

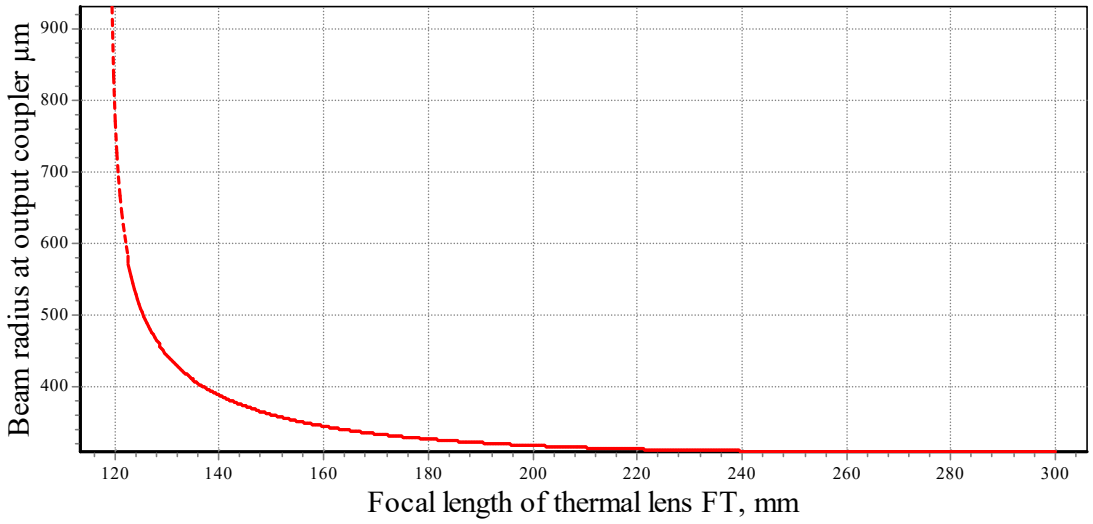

Figure 3.13: Beam radius at output coupler with respect to the focal length of the induced lens.

3.2.2.4 Semiconductor Saturable Absorber Mirror (SESAM)

The SESAM was procured from Batop GmbH, an optoelectronics company known for manufacturing SESAMs and other semiconductor components. Typically this nonlinear component consists of a Bragg-mirror on a semiconductor wafer like GaAs, with a thin absorber layer introduced in the top most Bragg-mirror layer pair as shown in figure 3.14. As the pulse hits the saturable absorber (which is a semiconductor with the bandgap energy that is smaller than the pulse photon energy) the electrons are excited to a higher energy state. As intensity of the pulse grows, a large number of electrons is excited thus saturating the absorber. So the pulse does not observe any loss at its peak and returns to the cavity. However, the pulse front side experiences absorption (it has lower intensity than the peak) thus shrinking the width of the pulse. Pulse back side also experiences absorption if the SESAM recovery time is faster compared to the pulse duration. At low intensities, the absorber is not saturated, and absorbs all incident energy, i.e. effectively removing all noise from the laser cavity and resulting in suppression of possible Q-switched mode-locking instabilities.

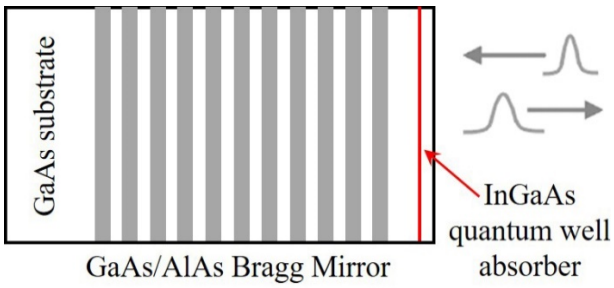

Figure 3.14: Structure of a typical SESAM for operation around 1064 nm.

To prevent SESAM from unwanted degradation and damage due to high pulse energies, its saturation fluence (energy density) must be low. To decrease the saturation fluence, the thickness of the semiconductor absorber layer is reduced to below ~10 nm. In this case a quantization of the electron energy and the momentum in the direction perpendicular to the absorber layer takes place and as a consequence the density of states decrease below the value

of a bulk semiconductor. Therefore the absorber layers in the SESAM are thin quantum wells with a smaller band gap than the barriers on both sides [83]. Parameters of the SESAM used in this experiment are listed in table 3.2.

Table 3.2: Parameters of the SESAM used in this experiment

Laser wavelength	λ	= 1064 nm
High reflection band (R > 98%)	λ	=1020 … 1100 nm
Modulation depth	ΔR	=6%
Non-saturable loss	A_{ns}	=6%
Saturation fluence	ϕ_{sat}	=70 μJ/cm^2
Relaxation time constant	τ	~1 ps
Damage threshold	ϕ	=3 mJ/cm^2
Chip area		4 mm x 4 mm
Chip thickness		450 μm
Protection		Protected with a dielectric front layer

Saturation intensity I_{sat} and saturation fluence E_{sat} influence the mode-locking build-up and the pulse stability with respect to self-Q-switching. Figure 3.15 shows saturation behavior of SESAM. Initially, the pulses are formed by noise fluctuations in the laser, and the saturation amount at this early stage is dominated by the CW intensity incident on the absorber [figure 3.15]. At the beginning, the saturable absorber is not fully bleached ($I << I_{sat}$).

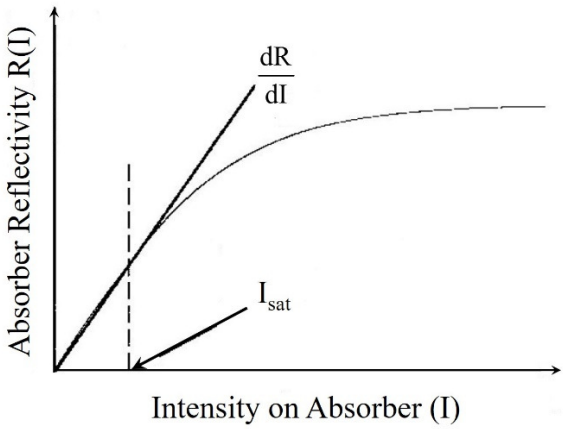

Figure 3.15: Nonlinear reflectivity change of a saturable absorber mirror due toabsorption bleaching with the CW intensity [79].

The slope dR/dI at around $I \approx 0$ determines the mode-locking build-up time and can be written as

$$T_{build-up} \propto \frac{1}{\left.\frac{dR}{dI}\right|_{I \approx 0} I} \tag{3.14}$$

Figure 3.15 shows that small intensity fluctuations will introduce a larger reflectivity change of the saturable absorber if the slope is larger. Therefore, the mode-locking build-up time decreases with smaller saturation intensities. However, there is a tradeoff: if the saturation intensity is too small, the laser will start to Q-switch. The condition for no Q-switching was derived in [84] as,

$$\text{Condition for no Q-switching: } \left|\frac{dR}{dI}\right| I < r\frac{T_R}{\tau_2} \tag{3.15}$$

where r is the pump parameter that determines how many times the laser is pumped above threshold τ_2 and is the upper state lifetime of the laser.

Chapter 4 Results and Discussion

In this chapter results and necessary discussions of the experiment are provided. Starting with quantum defect reduction, comments on CW operation, thermal lensing and pump absorption have been made. The chapter is concluded with the results of mode-locked regime and characterization of the generated pulses.

4.1 Quantum defect Reduction:

As mentioned in the motivation part, the main feature of this work was the mode-locked operation with low thermal lensing, which comes from the fact of having a low quantum defect in the system. The improvement of QD for a single photon is illustrated below:

At 810 nm pumping $QD_{810} = h\nu_{pump} - h\nu_{laser} = hc\left(\frac{1}{810nm} - \frac{1}{1067nm}\right) = 5.907\times10^{-20} J$

At 910 nm pumping $QD_{910} = h\nu_{pump} - h\nu_{laser} = hc\left(\frac{1}{910\,nm} - \frac{1}{1067\,nm}\right) = 3.212\times10^{-20} J$

Reduction in QD = $QD_{810} - QD_{910} = 2.695\times10^{-20} J$

So, 910 nm pumping in this case has reduced the quantum defect by more than 45%.

4.2 CW regime

The cavity was initially designed for the CW operation, where one HR end mirror was used instead of SESAM. The rest of the setup was unaltered, same fiber-coupled laser diode was occupied for pumping the crystal. In this way, 1 W of average output power was reached using a 1.6% output coupler when the absorbed power was 4.34 W. Optical power supplied to the crystal was 6.12 W, which corresponds to over 70% of pump absorbance and 24% optical to optical efficiency.

The laser radiation was polarized parallel to the N_m-axis. One distinguishing fact about the solid-state laser systems is that in a simple cavity they tend to produce nearly-diffraction limited beam. For output beam profiling a 125 mm focal length lens was used after the output coupler. To measure the beam quality factor, M^2, a CCD beam profiler was used to measure the spot sizes of the focused beam. For the continuous wave operation, the $M^2 < 1.2$ at the highest output power, when laser diode current was ~8 A, which corresponds to 13.4 W of incident pump power. An example of the beam quality measurement is shown in figure 4.1. The M^2 value and the beam waist W_0 of the laser beam were calculated by fitting the measured spot sizes to the Gaussian beam propagation equation which is given below,

$$W(z) = W_0\sqrt{1+\left(\frac{M^2 z\lambda_0}{n\pi W_0}\right)^2} \tag{4.1}$$

where, W_0 is the beam waist, λ_0 is the laser wavelength and z is the position of the beam along propagation axis.

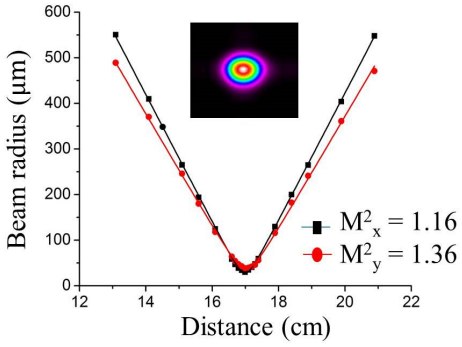

Figure 4.1: Beam quality of the CW Nd:KGW laser [24].

4.3 Thermal lensing

Pumping at longer wavelength comes with lower thermal lensing effects inside the crystal. The strength of thermal lensing for each pump power level was estimated by measuring the beam size variation away from the output coupler. After the laser beam waist was found

experimentally, a laser cavity with a variable lens inside the laser crystal was simulated using the ABCD matrix roundtrip model in LASCAD software. To find the power of thermal lensing, simulated lens inside the laser crystal was varied to match the exact focal power at which the beam waist from the simulated laser cavity model matches with the beam waist from the experimental measurement [85]. The following table shows that pumping at longer wavelength instead of standard wavelength can reduce the thermal lensing power by a factor of ~2 for Nd:KGW crystal in CW regime [24].

Table 4.1: Thermal lensing variation with pump wavelength change

Author	Pump wavelength (nm)	Absorbed power (W)	Thermal lens power (D)
H. Ke *et al.* [86]	808	2.6	9.5
H. Ke *et al.* [86]	877	4.3	9.5
This work	910	8.3	5.7

4.4 Pump Absorption

Although absorption cross-section of hot-band pump transition employed in this work is in general fairly weak [17, 37], the pump absorption in the Nd:KGW crystal at 910 nm pump wavelength was measured to be up to 50-70%. It depended on the pump power level owing to the pump wavelength shift with drive current. In figure 4.2 (a), black line represents fluorescence of 3 at.% Nd:KGW and the red line is spectrum of fiber-coupled laser diode. In this experiment pump absorption coefficient at 910 nm was calculated to be 0.6 cm^{-1}. From the figure 4.2 (b) we observe that the pump power absorption is almost linear with the input pump power. The pump power intensity at the crystal end-face was calculated to be 3.6 KW/cm^2 and no crystal fracture was observed

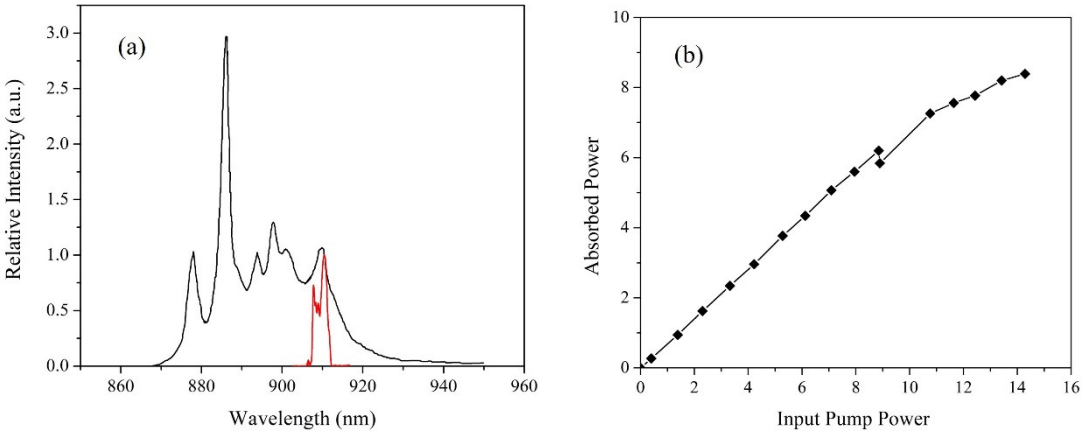

Figure 4.2: (a) Fluorescence spectra of Nd:KGW (black line) [17] and emission spectrum of the pump laser diode (red line). (b) Absorbed pump power vs input pump power.

4.5 Mode-locked regime

4.5.1 Q-switched instabilities

The input-output power performance of the designed laser with the SESAM in the cavity is displayed in figure 4.4. The laser exhibited two separate regimes of operation. As the HR end mirror was replaced by SESAM, the cavity started producing large envelops of pulses with inconsistent amplitude. Below 5 W of absorbed pump power the Q-switched mode-locked regime was observed as shown in figure 4.3(a).

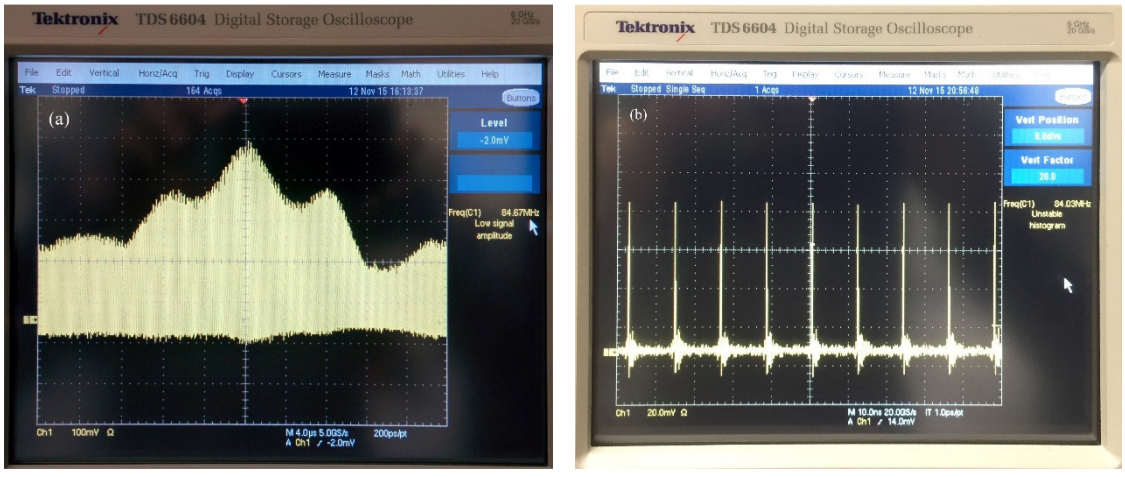

Figure 4.3: (a) Unstable mode-locking below 5 W of absorbed power; (b) stable pulse train above 5 W of absorbed power.

Above that point, stable mode-locked pulse train was routinely generated with a period of cavity roundtrip time as shown in 4.3 (b). This behavior can be explained by the fact that individual laser pulses already had enough energy to completely saturate the SESAM.

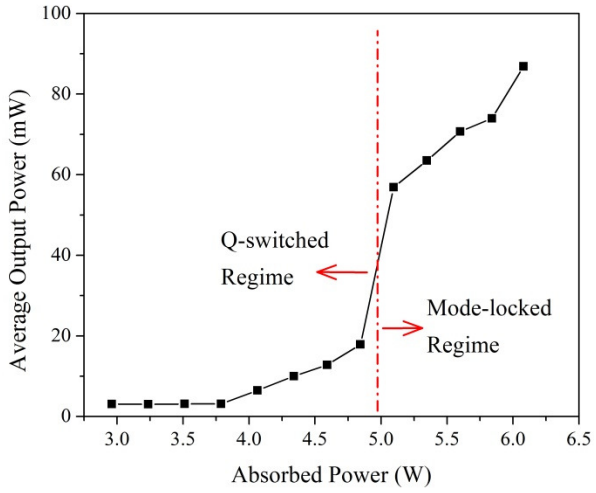

Figure 4.4: The measured output power.

At the onset of the mode-locked regime a sudden jump in the output power was observed as shown in figure 4.4. This can be interpreted as a full saturation of the SESAM by the generated pulses, which bleached its saturable losses (i.e. modulation depth) of 6%. For 6.08 W of absorbed pump power, 2.4 ps long pulses were obtained at 87 mW of average output power. The high level of intracavity loss (~6%) introduced by the SESAM contributed to the moderate output power as compared to the CW regime.

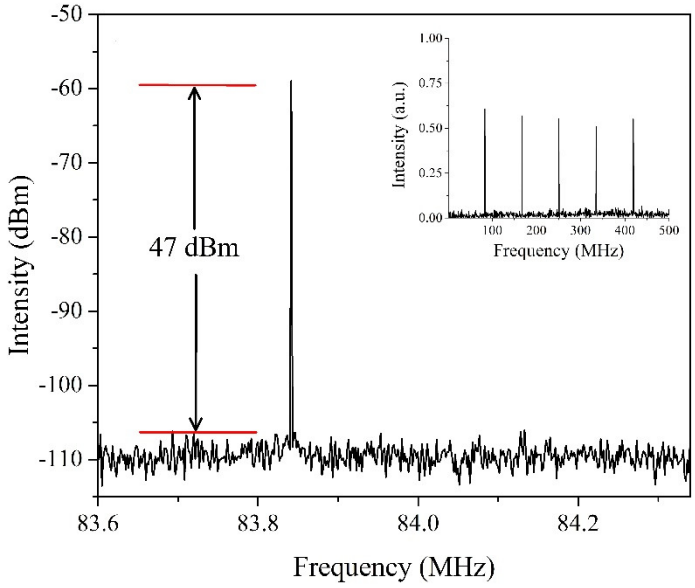

Figure 4.5: RF spectrum of the fundamental mode at ~83.8 MHz. Inset: wide span RF spectrum.

The radio frequency (RF) spectrum of the mode-locked laser is shown in figure 4.5. The spectral power of the fundamental mode was 47 dBm above the noise level. In a wide-range RF scan measurement (inset in figure 4.5), no additional peaks between the higher order modes were observed indicating stable single-pulse mode-locking without Q-switching instabilities.

4.5.2 Characterization of single pulsed regime

The autocorrelation trace of the output pulses was acquired with a commercially available long range (~200 ps) auto-correlator (Femtochrome, FR-103XL) and is shown in the following figure 4.6. The pulse duration and output spectrum bandwidth was measured with an oscilloscope and processed with Origin software. The bandwidth of the output spectrum (also shown in figure 4.6) at FWHM was found to be 0.74 nm. In continuous wave regime the output spectrum bandwidth was 0.13 nm, which increased to 0.74 nm due to mode-locking (i.e. generation and locking of longitudinal frequency modes). The longer time ranges were monitored with a fast photodiode and an oscilloscope with combined resolution of ~ 100 ps.

Assuming *sech*^{2} temporal shape, the typical pulse duration at the output of the laser was determined to be 2.4 ps.

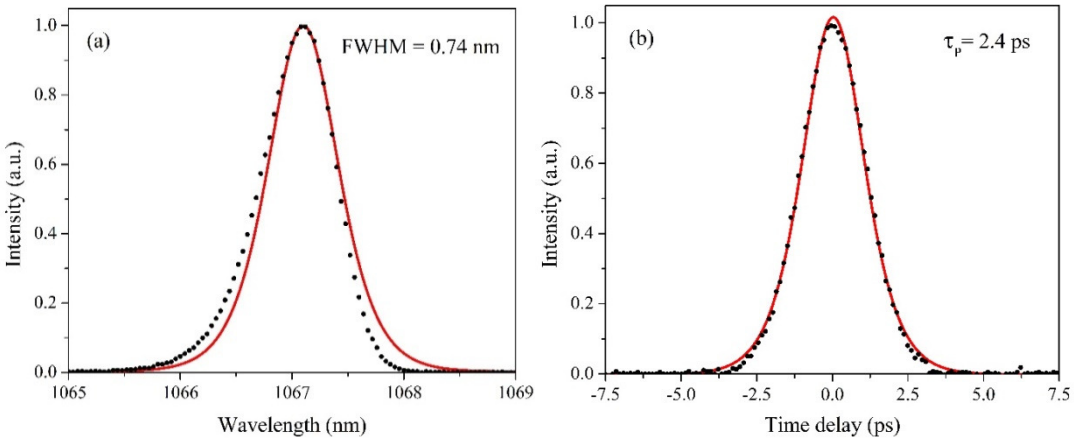

Figure 4.6 The spectrum (a) and the intensity autocorrelation (b) of the generated pulses. Red solid lines indicate corresponding *sech*^{2} shape fits.

The time-bandwidth product was calculated to be

$$\mathrm{TBWP} = \Delta\tau \times \Delta\lambda \times \frac{c}{\lambda^2} = 2.4\mathrm{ps} \times 0.74\mathrm{nm} \times \frac{3*10^8}{(1067\mathrm{nm})^2} = 0.44$$

which deviates from the transform-limited one (0.315 for *sech*^{2}) as expected in the positive dispersion mode-locking regime. The average output power was 87 mW, at a repetition rate of ~83.8 MHz which translates to a pulse energy of,

$$E_{pulse} = \frac{\text{average O/P power}}{\text{Repetition rate}} = \frac{87\ \text{mW}}{83.8\ \text{MHz}} \cong 1\ \text{nJ}$$

The peak power of the generated pulses was calculated as per following,

$$P_{peak} = \frac{\text{average O/P power}}{\text{Repetition rate} \times \text{Pulse duration}} = \frac{87\ \text{mW}}{83.8\ \text{MHz} \times 2.4\ \text{ps}} \cong 427\ \text{W}$$

The time required for a pulse to take a roundtrip through the cavity was also calculated as the inverse of the repetition rate found from the RF measurements. This means that in the pulse train the pulses are spaced by the following time:

$$T_{roundtrip} = \frac{1}{Repetition\ \ rate} = \frac{1}{\sim 83.8\ \text{MHz}} \cong 11\ \text{ns}$$

The output beam quality was measured for the continuous wave operation and it was found to be nearly diffraction limited (see figure 4.7) and the beam quality factor M^2 was found to be less than 1.18.

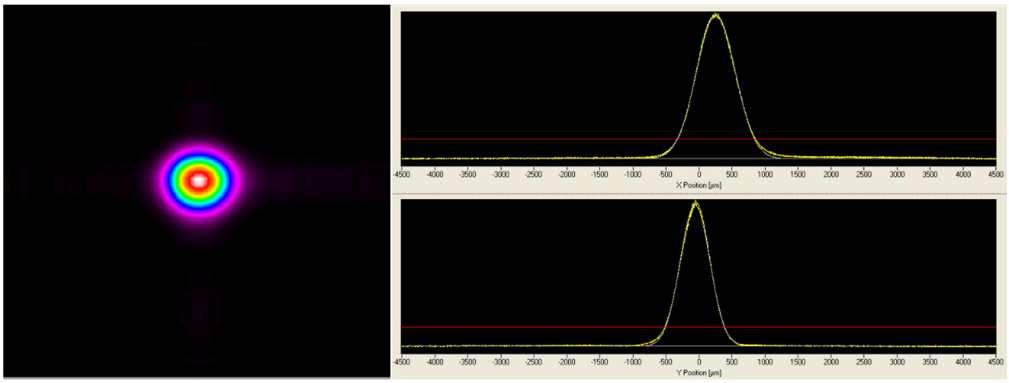

Figure 4.7: Spatial beam profile with corresponding Gaussian intensity fits in the vertical and horizontal directions.

The SESAM fluence required to saturate the absorption was $70\ \mu J/cm^2$. In the experiment the output pulse energy was $1\ nJ$ with 1.6% output coupler, which translates into 62.5 nJ of intracavity pulse energy. The beam spot size diameter at SESAM was $131\ \mu m$. From these data the fluence on SESAM was calculated to be $\approx 470\ \mu J/cm^2$ which is high enough to saturate absorption of SESAM (typically we need >5 times the saturation fluence) [79].

From literature, diode end-pumped Nd:$Gd_{0.5}Y_{0.5}VO_4$ was passively mode-locked in a folded cavity produced 3.8 ps pulses at 3.9 W of average output energy [87]. Simple 3 mirror cavity setup along with SESAM as one of the end mirror resulted in higher output power. Similar cavity setup with Nd:YVO_4 crystal produced 2.1 ps pulses at 1.28 W of average output power [88].

Chapter 5 Conclusion & Future work

In this chapter final remarks on this experimental work are presented.

5.1 Conclusion

A laser-diode end pumped mode-locked Nd:KGW laser was constructed in the laboratory. We have demonstrated passive mode-locking of a Nd:KGW laser hot-band-pumped at 910 nm. A semiconductor saturable absorber mirror was used to generate 2.4 ps pulses at a repetition rate of ~83.8 MHz. An output power of 87 mW was obtained at 1067 nm. This is the first report of mode-locking performance observed with hot-band pumping in Nd:KGW laser. At the same time the generated pulses are the shortest reported to date for SESAM mode-locked Nd:KGW lasers. Low quantum defect pumping at 910 nm opens the way for further output power scaling due to the reduced influence of thermal effects.

5.2 Future work

Nd:KGW crystal is widely used for self-Raman lasers. There is no demonstration of continuous wave operation producing ultrashort light pulses from the Nd-doped self-Raman laser crystals in the eye safe spectral range. In a new cavity, we will try to operate the Nd:KGW laser at 1350 nm in continuous wave regime. By utilizing a high power laser diode at 910 nm, strong intracavity laser intensity at the crystal will be created to fulfill the conditions for Raman wavelength shift. Later incorporating proper optics, steps will be taken to operate this self-Raman laser in the mode-locked regime to generate ultrashort pulses at ~1540 nm. On the other hand, a SESAM with lower insertion loss can be used to achieve higher output power at 1067 nm or 1350 nm.

Appendix A Gaussian Beam in Cavity

The transfer matrices of different cavity elements are given by:

Table 5.1: Transfer matrices for different optical elements

Propagation in free space	$\begin{bmatrix} 1 & \mathrm{d} \\ 0 & 1 \end{bmatrix}$	d is the distance
Propagation in the crystal	$\begin{bmatrix} 1 & \mathrm{l_c/n} \\ 0 & 1 \end{bmatrix}$	l_c is the crystal length n is the refractive index
Reflection from flat mirror	$\begin{bmatrix} 1 & 0 \\ 0 & 1 \end{bmatrix}$	
Reflection from concave mirror	$\begin{bmatrix} 1 & 0 \\ 2/\mathrm{r} & 1 \end{bmatrix}$	r is the radius of curvature, $r < 0$
Thermal or Kerr lens	$\begin{bmatrix} 1 & 0 \\ -2/\mathrm{f} & 1 \end{bmatrix}$	f is the focal length, $f > 0$

For a general optical beam, it is possible to define a generalized complex radius of curvature q, such that this q parameter follows the same propagation rule as the complex radius of a Gaussian beam propagating in the same arbitrary ABCD optical system. The real radius of curvature R is related to the mean radius of curvature of the phase front, while the real beam size W is related to the second order moment of the intensity. The beam quality factor M^2 multiplies the wavelength λ in the defining equation [89]:

$$\frac{1}{\mathrm{q}} = \frac{1}{\mathrm{R}} - j\frac{\mathrm{M}^2\lambda}{\pi \mathrm{w}^2} \tag{5.1}$$

A transformation of Gaussian beams as it passes through an optical system is given by:

$$\mathrm{q}_2 = \frac{\mathrm{A}\mathrm{q}_1 + \mathrm{B}}{\mathrm{C}\mathrm{q}_1 + \mathrm{D}} \tag{5.2}$$

For an arbitrary beam to evolve into a stable steady-state beam, the beam profiles at the mirrors must duplicate itself after successive passes through the cavity. Equation (1) presents the relationship of beam parameter q as a function of distance z within the cavity to any optical element. Roundtrip matrix is found by multiplying each elements of the ABCD matrix starting and ending at the same point.

$$q_1(z) = \frac{Aq_1(z) + B}{Cq_1(z) + D} \tag{5.3}$$

By solving this equation and comparing with the cited equation, the beam radius and the wave front curvature can be defined and found as:

$$w^2 = \frac{\lambda|B|/\pi}{\sqrt{1-(D+A/2)^2}} \tag{5.4}$$

$$R = \frac{2B}{D-A} \tag{5.5}$$

Now from the equation above, in the denominator the squared term must be greater than unity to have a positive and real beam radius w to establish a stable cavity; this is called the cavity stability condition.

$$\left(\frac{A+D}{2}\right)^2 \le 1 \Rightarrow -1 \le \left(\frac{A+D}{2}\right) \le 1 \tag{5.6}$$

The following parameters were found from this study:

$$A = -0.398; B = 268.334; C = -0.004; D = 0.358$$

In order to calculate the mode size inside the gain medium Eq. 2 can be used where λ=1067 nm

$$w = \sqrt{\frac{\lambda|B|/\pi}{\sqrt{1-\left(\frac{D+A}{2}\right)^2}}} = \sqrt{\frac{1067\times10^{-6}\times268.334/\pi}{\sqrt{1-\left(\frac{0.358-0.398}{2}\right)^2}}} = 301.91\ \mu m$$

References

[1] Maiman, T.H., 1960. Stimulated optical radiation in ruby.

[2] Akbari, R. and Major, A., 2013. Optical, spectral and phase-matching properties of BIBO, BBO and LBO crystals for optical parametric oscillation in the visible and near-infrared wavelength ranges. *Laser Physics*, *23*(3), p.035401.

[3] Zhao, H., Lima Jr, I.T. and Major, A., 2010. Near-infrared properties of periodically poled $KTiOPO_4$ and stoichiometric MgO-doped $LiTaO_3$ crystals for high power optical parametric oscillation with femtosecond pulses. *Laser Physics*, *20*(6), pp.1404-1409.

[4] Major, A., Sandkuijl, D. and Barzda, V., 2009. Efficient frequency doubling of a femtosecond Yb:KGW laser in a BiB_3O_6 crystal. *Optics express*, *17*(14), pp.12039-12042.

[5] Lima Jr, I.T., Kultavewuti, V. and Major, A., 2010. Phasematching properties of congruent MgO-doped and undoped periodically poled $LiNbO_3$ for optical parametric oscillation with ultrafast excitation at 1 μm. *Laser Physics*, *20*(1), pp.270-275.

[6] Sandkuijl, D., Cisek, R., Major, A. and Barzda, V., 2010. Differential microscopy for fluorescence-detected nonlinear absorption linear anisotropy based on a staggered two-beam femtosecond Yb:KGW oscillator. *Biomedical optics express*, *1*(3), pp.895-901.

[7] Nikolakakos, I.P., Major, A., Aitchison, J.S. and Smith, P.W., 2004. Broadband characterization of the nonlinear optical properties of common reference materials. *IEEE Journal of selected topics in quantum electronics*, *10*(5), pp.1164-1170.

[8] Major, A., Yoshino, F., Aitchison, J.S., Smith, P.W., Sorokin, E. and Sorokina, I.T., 2004. Ultrafast nonresonant third-order optical nonlinearities in ZnSe for photonic switching at telecom wavelengths. *Applied physics letters*, *85*(20), pp.4606-4608.

[9] Syage, J.A., Felker, P.M. and Zewail, A.H., 1984. Picosecond dynamics and photoisomerization of stilbene in supersonic beams. II. Reaction rates and potential energy surface. *The Journal of chemical physics*, *81*(11), pp.4706-4723.

[10] Hentschel, M., Kienberger, R., Spielmann, C., Reider, G.A., Milosevic, N., Brabec, T., Corkum, P., Heinzmann, U., Drescher, M. and Krausz, F., 2001. Attosecond metrology. *Nature*, *414*(6863), pp.509-513.

[11] Graf, T. and Balmer, J.E., 1995. Lasing properties of diode-laser-pumped Nd:KGW. *Optical Engineering*, *34*(8), pp.2349-2352.

[12] Huang, K., Ge, W.Q., Zhao, T.Z., Feng, C.Y., Yu, J., He, J.G., Xiao, H. and Fan, Z.W., 2016. High-power passively Q-switched Nd:KGW laser pumped at 877 nm. *Applied Physics B*, *122*(6), pp.1-7.

[13] Major, A., Langford, N., Graf, T., Burns, D. and Ferguson, A.I., 2002. Diode-pumped passively mode-locked Nd:$KGd(WO_4)_2$ laser with 1-W average output power. *Optics letters*, *27*(16), pp.1478-1480.

[14] Major, A., Langford, N., Graf, T. and Ferguson, A.I., 2002. Additive-pulse mode-locking of a diode-pumped Nd:$KGd(WO_4)_2$ laser. *Applied Physics B*, *75*(4-5), pp.467-469.

[15] Koechner, W. and Bass, M., 2003. *Solid-State Lasers: A Graduate Text*. Springer Science & Business Media.

[16] Yumashev, K.V., Savitski, V.G., Kuleshov, N.V., Pavlyuk, A.A., Molotkov, D.D. and Protasenya, A.L., 2007. Laser performance of N_g-cut flash-lamp pumped Nd:KGW at high repetition rates. *Applied Physics B*, *89*(1), pp.39-43.

[17] Moncorgé, R., Chambon, B., Rivoire, J.Y., Garnier, N., Descroix, E., Laporte, P., Guillet, H., Roy, S., Mareschal, J., Pelenc, D. and Doury, J., 1997. Nd doped crystals for medical laser applications. *Optical Materials*, *8*(1), pp.109-119.

[18] Kaminskii, A.A., Pavlyuk, A.A., Klevtsov, P.V., Balashov, I.F., Berenberg, V.A., Sarkisov, S.E., Fedorov, V.A., Petrov, M.V. and Lyubchenko, V.V., 1977. Stimulated radiation of monoclinic crystals of $KY(WO_4)_2$ and $KGd(WO_4)_2$ with Ln^{3+} ions. *Inorganic Materials*, *13*(3), pp.482-483.

[19] Major, A., Aitchison, J.S., Smith, P.W., Druon, F., Georges, P., Viana, B. and Aka, G.P., 2005. Z-scan measurements of the nonlinear refractive indices of novel Yb-doped laser crystal hosts. *Applied Physics B*, *80*(2), pp.199-201.

[20] Major, A., Nikolakakos, I., Aitchison, J.S., Ferguson, A.I., Langford, N. and Smith, P.W.E., 2003. Characterization of the nonlinear refractive index of the laser crystal Yb:$KGd(WO_4)_2$. *Applied Physics B*, *77*(4), pp.433-436.

[21] Major, A., Aitchison, J.S., Smith, P.W., Langford, N. and Ferguson, A.I., 2005. Efficient Raman shifting of high-energy picosecond pulses into the eye-safe 1.5-μm spectral region by use of a $KGd(WO_4)_2$ crystal. *Optics letters*, *30*(4), pp.421-423.

[22] Hönninger, C., Paschotta, R., Morier-Genoud, F., Moser, M. and Keller, U., 1999. Q-switching stability limits of continuous-wave passive mode-locking. *JOSA B*, *16*(1), pp.46-56.

[23] Mochalov, I.V., 1997. Laser and nonlinear properties of the potassium gadolinium tungstate laser crystal $KGd(WO_4)_2$: Nd^{3+}-(KGW:Nd). *Optical Engineering*, *36*(6), pp.1660-1669.

[24] Talukder, R.C., Halim, M.Z., Waritanant, T. and Major, A., 2016. Multiwatt continuous wave Nd:KGW laser with hot-band diode pumping. *Optics Letters 41*(16), pp.3810-3812.

[25] Bui, A.A., Dashkevich, U.I., Orlovich, V.A. and Khodasevich, I.A., 2015. Diode-Pumped Nd:$KGd(WO_4)_2$ Laser: Lasing at Fundamental and Second Harmonic Frequencies. *Journal of Applied Spectroscopy*, *82*(4), pp.578-584.

[26] Halim, M.Z., Talukder, R.C., Waritanant, T. and Major, A., 2016. Passive mode-locking of Nd:KGW laser with hot band diode pumping. In *2016 Photonics North*, pp. 1-1. IEEE.

[27] Eibna Halim, M.Z., Talukder, R.C., Waritanant, T. and Major, A., 2016. Passive mode locking of a Nd:KGW laser with hot-band diode pumping. *Laser Physics Letters*, *13*(10), p.105003.

[28] Laser Crystal Solutions, [Online]. Available: http://www.lc-solutions.com/product/ndkgw.php. [Accessed 05-09-2016]

[29] Stetser, D.A. and DeMaria, A.J., 1966. Optical spectra of ultrashort optical pulses generated by mode-locked glass: Nd lasers. *Applied Physics Letters*, *9*(3), pp.118-120.

[30] Fluck, R., Weingarten, K.J., Moser, M., Zhang, G. and Keller, U., 1996. Diode-pumped passively mode-locked 1.3-μm Nd:YVO_4 and Nd:YLF lasers by use of semiconductor saturable absorbers. *Optics letters*, *21*(17), pp.1378-1380.

[31] Spühler, G.J., Südmeyer, T., Paschotta, R., Moser, M., Weingarten, K.J. and Keller, U., 2000. Passively mode-locked high-power Nd:YAG lasers with multiple laser heads. *Applied Physics B*, *71*(1), pp.19-25.

[32] Zellmer, H., Unger, S., Albers, P., Reichel, V., Willamowski, U., Tünnermann, A., Müller, H.R., Kirchhof, J. and Welling, H., 1995. High-power cw neodymium-doped fiber laser operating at 9.2 W with high beam quality. *Optics letters*, *20*(6), pp.578-580.

[33] Lamb, K., Spence, D.E., Hong, J., Yelland, C. and Sibbett, W., 1994. All-solid-state self-mode-locked Ti: sapphire laser. *Optics letters*, *19*(22), pp.1864-1866.

[34] Ghanbari, S., Akbari, R. and Major, A., 2016. Femtosecond Kerr-Lens Mode-Locked Alexandrite Laser. *Optics Express 24*(13), pp.14836-14840.

[35] Musset, O. and Boquillon, J.P., 1997. Comparative laser study of Nd:KGW and Nd:YAG near 1.3 μm. *Applied Physics B*, *64*(4), pp.503-506.

[36] Eksma Optics, [Online]. http://eksmaoptics.com/nonlinear-and-laser-crystals/laser-crystals/nd-kgw-crystals/. [Accessed 05-09-2016].

[37] Loiko, P., Yoon, S.J., Serres, J.M., Mateos, X., Beecher, S.J., Birch, R.B., Savitski, V.G., Kemp, A.J., Yumashev, K., Griebner, U. and Petrov, V., 2016. Temperature-dependent spectroscopy and microchip laser operation of Nd:$KGd(WO_4)_2$. *Optical Materials*, *58*, pp.365-372.

[38] Kushawaha, V., Michael, A. and Major, L., 1994. Effect of Nd concentration on the Nd:KGW laser. *Applied Physics B*, *58*(6), pp.533-535.

[39] Major, A., Sukhoy, K., Zhao, H. and Lima Jr, I.T., 2011. Green sub-nanosecond microchip laser based on BiBO crystals. *Laser Physics*, *21*(1), pp.57-60.

[40] Zhao, H., Sukhoy, K., Lima Jr, I.T. and Major, A., 2012. Generation of green second harmonic with 60% conversion efficiency from a Q-switched microchip laser in MgO: PPLN crystal. *Laser Physics Letters*, *9*(5), p.355.

[41] Kushawaha, V., Banerjee, A. and Major, L., 1993. High-efficiency flashlamp-pumped Nd:KGW laser. *Applied Physics B*, *56*(4), pp.239-242.

[42] Gulev, V.S., Pavlyuk, A.A., Kozeeva, L.P. and Nesterenko, V.F., 1990. Lasers on the basis of the double molybdates and tungstates. In *OE/LASE 1990,* pp. 103-114. International Society for Optics and Photonics.

[43] Kaminskiĭ, A.A., Verdún, H.R., Koechner, W., Kuznetsov, F.A. and Pavlyuk, A.A., 1992. Efficient single-mode cw lasers based on monoclinic double potassium-(rare earth) tungstenate crystals containing Nd^{3+} ions with semiconductor-laser pumping. *Quantum Electronics*, *22*(10), pp.875-877.

[44] Chen, Y., Lin, Y., Gong, X., Tan, Q., Zhuang, J., Luo, Z. and Huang, Y., 2007. Polarized spectroscopic properties of Nd^{3+}-doped $KGd(WO^4)^2$ single crystal. *Journal of luminescence*, *126*(2), pp.653-660.

[45] Lee, A.J., Pask, H.M., Spence, D.J. and Piper, J.A., 2010, January. Generation of yellow, continuous-wave emission from an intracavity, frequency-doubled Nd:KGW

self-Raman laser. In *Advanced Solid-State Photonics* (p. ATuA22). Optical Society of America.

[46] Demidovich, A.A., Grabtchikov, A.S., Lisinetskii, V.A., Burakevich, V.N., Orlovich, V.A. and Kiefer, W., 2005. Continuous-wave Raman generation in a diode-pumped Nd^{3+}:$KGd(WO_4)_2$ laser. *Optics letters*, *30*(13), pp.1701-1703.

[47] Tang, C.Y., Zhuang, W.Z., Su, K.W. and Chen, Y.F., 2015. Efficient Continuous-Wave Self-Raman Nd:KGW Laser With Intracavity Cascade Emission Based on Shift of 89 cm^{-1}. *IEEE Journal of Selected Topics in Quantum Electronics*, *21*(1), pp.142-147.

[48] Piper, J.A. and Pask, H.M., 2007. Crystalline Raman lasers. *IEEE Journal of Selected Topics in Quantum Electronics*, *13*(3), pp.692-704.

[49] Grabtchikov, A.S., Kuzmin, A.N., Lisinetskii, V.A., Ryabtsev, G.I., Orlovich, V.A. and Demidovich, A.A., 2000. Stimulated Raman scattering in Nd:KGW laser with diode pumping. *Journal of alloys and compounds*, *300*, pp.300-302.

[50] Jakutis-Neto, J., Lin, J., Wetter, N.U. and Pask, H., 2012. Continuous-wave watt-level Nd:YLF/KGW Raman laser operating at near-IR, yellow and lime-green wavelengths. *Optics express*, *20*(9), pp.9841-9850.

[51] Savitski, V.G., Friel, I., Hastie, J.E., Dawson, M.D., Burns, D. and Kemp, A.J., 2012. Characterization of single-crystal synthetic diamond for multi-watt continuous-wave Raman lasers. *IEEE Journal of Quantum Electronics*, *48*(3), pp.328-337.

[52] Savitski, V.G., 2014. Experimental analysis of emission linewidth narrowing in a pulsed $KGd(WO_4)_2$ Raman laser. *Optics express*, *22*(18), pp.21767-21774.

[53] Chang, M.T., Zhuang, W.Z., Su, K.W., Yu, Y.T. and Chen, Y.F., 2013. Efficient continuous-wave self-Raman Yb:KGW laser with a shift of 89 cm^{-1}. *Optics express*, *21*(21), pp.24590-24598.

[54] Kurbasov, S.V. and Losev, L.L., 1999. Raman compression of picosecond microjoule laser pulses in $KGd(WO_4)_2$ crystal. *Optics communications*, *168*(1), pp.227-232.

[55] Grabtchikov, A.S., Kuzmin, A.N., Lisinetskii, V.A., Orlovich, V.A., Demidovich, A.A., Yumashev, K.V., Kuleshov, N.V., Eichler, H.J. and Danailov, M.B., 2001. Passively Q-switched 1.35 μm diode pumped Nd:KGW laser with V:YAG saturable absorber. *Optical Materials*, *16*(3), pp.349-352.

[56] Liu, M., Liu, J., Liu, S., Li, L., Chen, F. and Wang, W., 2009. Experimental study on passively Q-switched mode-locking diode-pumped Nd:KGW laser with Cr^{4+}:YAG. *Laser physics*, *19*(5), pp.923-926.

[57] Kalisky, Y., Kravchik, L. and Labbe, C., 2001. Repetitive modulation and passively Q-switching of diode-pumped Nd:KGW laser. *Optics communications*, *189*(1), pp.113-125.

[58] Flood, C.J., Walker, D.R. and Van Driel, H.M., 1995. CW diode pumping and FM mode-locking of a Nd:KGW laser. *Applied Physics B*, *60*(2-3), pp.309-312.

[59] Sweetser, J., Dunn, T.J., Palese, S., Walmsley, I.A., Radzewicz, C. and Miller, R.D., 1993. Efficient high repetition rate synchronous amplification of a passively mode-locked femtosecond dye laser. *Applied optics*, *32*(24), pp.4471-4479.

[60] Lettenberger, M., and K. Wolfrum. "Optimized Kerr lens mode-locking of a pulsed Nd:KGW laser." *Optics communications* 131, no. 4 (1996): 295-300.

[61] Major, A., Giniūnas, L., Langford, N., Ferguson, A.I., Burns, D., Bente, E.A.J.M. and Danielius, R., 2002. Saturable Bragg reflector-based continuous-wave mode-locking of Yb:$KGd(WO_4)_2$ laser. *Journal of Modern Optics*, *49*(5-6), pp.787-793.

[62] Zhao, H. and Major, A., 2013. Powerful 67 fs Kerr-lens mode-locked prismless Yb:KGW oscillator. *Optics express*, *21*(26), pp.31846-31851.

[63] Zhao, H. and Major, A., 2014. Megawatt peak power level sub-100 fs Yb:KGW oscillators. *Optics express*, *22*(25), pp.30425-30431.

[64] Akbari, R., Zhao, H., Fedorova, K.A., Rafailov, E.U. and Major, A., 2016. Quantum-dot saturable absorber and Kerr-lens mode-locked Yb:KGW laser with >450 kW of peak power. *Optics Letters 41*(16), pp.3771-3774.

[65] Sato, Y., Taira, T., Pavel, N. and Lupei, V., 2003. Laser operation with near quantum-defect slope efficiency in Nd:YVO_4 under direct pumping into the emitting level. *Applied physics letters*, *82*(6), pp.844-846.

[66] Risk, W.P., 1988. Modeling of longitudinally pumped solid-state lasers exhibiting reabsorption losses. *JOSA B*, *5*(7), pp.1412-1423.

[67] Sangla, D., Castaing, M., Balembois, F. and Georges, P., 2009. Highly efficient Nd:YVO_4 laser by direct in-band diode pumping at 914 nm. *Optics letters*, *34*(14), pp.2159-2161.

[68] Waritanant, T. and Major, A., 2016. High efficiency passively mode-locked Nd:YVO_4 laser with direct in-band pumping at 914 nm. *Optics Express*, *24*(12), pp.12851-12855.

[69] Ma, J.L., Xiong, B., Guo, L., Zhao, P.F., Zhang, L., Lin, X.C., Li, J.M. and Duanmu, Q.D., 2010. Low heat and high efficiency Nd:$GdVO_4$ laser pumped by 913 nm. *Laser Physics Letters*, *7*(8), pp.579-582.

[70] Kaminskii, A., P. Klevtsov, Lyudmila Li, and A. Pavlyuk. "Laser $^4F_{3/2} \rightarrow {}^4I_{9/2}$ and $^4F_{3/2} \rightarrow {}^4I_{13/2}$ transitions in $KY(WO_4)_2:Nd^{3+}$." *IEEE Journal of Quantum Electronics* 8, no. 5 (1972): 457-459.

[71] Lupei, V., Pavel, N. and Taira, T., 2002. Efficient laser emission in concentrated Nd laser materials under pumping into the emitting level. *IEEE journal of quantum electronics*, *38*(3), pp.240-245.

[72] Waritanant, T. and Major, A., 2016. Thermal lensing in Nd:YVO_4 laser with in-band pumping at 914 nm. *Applied Physics B*, *122*(5), pp.1-4.

[73] Andrew, M., 2009. Ultrafast Optics.

[74] Gürs, K. and Müller, R., 1963. Breitband-modulation durch steuerung der emission eines optischen masers (Auskoppelmodulation). *Physics Letters*, *5*(3), pp.179-181.

[75] Gürs, K., 1964. Beats and modulation in optical ruby-masers. In *Quantum Electronics, 1*, p. 1113.

[76] Statz, H. and Tang, C.L., 1964. Zeeman Effect and Nonlinear Interactions between Oscillating Modes in Masers. In *Quantum Electronics*, *1*, p. 469.

[77] Haus, H.A., 2000. Mode-locking of lasers. *IEEE Journal of Selected Topics in Quantum Electronics*, *6*(6), pp.1173-1185.

[78] Zhao, H., 2013. PhD thesis. Powerful diode-pumped ultrafast solid-state laser oscillators based on bulk Yb:$KGd(WO_4)_2$ crystals.

[79] Keller, U., Weingarten, K.J., Kartner, F.X., Kopf, D., Braun, B., Jung, I.D., Fluck, R., Honninger, C., Matuschek, N. and Der Au, J.A., 1996. Semiconductor saturable absorber mirrors (SESAM's) for femtosecond to nanosecond pulse generation in solid-state lasers. *IEEE Journal of selected topics in Quantum Electronics*, *2*(3), pp.435-453.

[80] D. R. Paschotta, "Bulk Lasers," [Online]. Available: https://www.rp-photonics.com/bulk_lasers.html. [Accessed 05-09-2016].

[81] Loiko, P.A., Denisov, I.A., Yumashev, K.V., Kuleshov, N.V. and Pavlyuk, A.A., 2010. Laser performance and thermal lensing in flashlamp pumped N_p-cut and N_g-cut Nd:KGW crystals. *Applied Physics B*, *100*(3), pp.477-483.

[82] Loiko, P.A., Yumashev, K.V., Kuleshov, N.V., Savitski, V.G., Calvez, S., Burns, D. and Pavlyuk, A.A., 2009. Thermal lens study in diode pumped N_g-and N_p-cut Nd:$KGd(WO_4)_2$ laser crystals. *Optics express*, *17*(26), pp.23536-23543.

[83] "How does SAM work?," Batop Optoelectronics , [Online]. Available: http://www.batop.de/information/SAM_infos.html. [Accessed 05-09-2016].

[84] Kaertner, F.X., Brovelli, L.R., Kopf, D., Kamp, M., Calasso, I.G. and Keller, U., 1995. Control of solid state laser dynamics by semiconductor devices. *Optical Engineering*, *34*(7), pp.2024-2036.

[85] H. Mirzaeian, S. Manjooran and A. Major, "A simple technique for accurate characterization of thermal lens in solid state lasers," Proceedings of SPIE 9288, 928802 (2014).

[86] Huang, K., Ge, W.Q., Zhao, T.Z., He, J.G., Feng, C.Y. and Fan, Z.W., 2015. Comparative study of Nd:KGW lasers pumped at 808 nm and 877 nm. In *Applied Optics and Photonics China,* pp. 96711W-96711W. International Society for Optics and Photonics.

[87] He, J.L., Fan, Y.X., Du, J., Wang, Y.G., Liu, S., Wang, H.T., Zhang, L.H. and Hang, Y., 2004. 4-ps passively mode-locked Nd:$Gd_{0.5}Y_{0.5}VO_4$ laser with a semiconductor saturable-absorber mirror. *Optics letters*, *29*(23), pp.2803-2805.

[88] Fan, Y.X., He, J.L., Wang, Y.G., Liu, S., Wang, H.T. and Ma, X.Y., 2005. 2-ps passively mode-locked Nd:YVO_4 laser using an output-coupling-type semiconductor saturable absorber mirror. *Applied Physics Letters*, *86*(10).

[89] Bélanger, P.A., 1991. Beam propagation and the ABCD ray matrices. *Optics Letters*, *16*(4), pp.196-198.